

Multisite Amino-Allylidene Ligands from Thermal CO Elimination in Diiron Complexes and Catalytic Activity in Hydroboration Reactions

Chiara Zappelli,^[a] Francesco Taglieri,^[b] Silvia Schoch,^[a] Giulio Bresciani,^[a] Tiziana Funaioli,^[a] Fabio Marchetti,^{*,[a]} Stefano Zacchini,^[c] Andrea Di Giuseppe,^{*,[b]} and Marcello Crucianelli^{*,[b]}

The new diiron(I) complexes $[\text{Fe}_2\text{Cp}_2(\mu\text{-CO})\{\mu\text{-}k^3\text{C}_k\text{N-C}(\text{R}^1)\text{C}(\text{R}^2)\text{C}(\text{CN})\text{NMe}(\text{R})\}]$, **3a–o** (R = alkyl or 4-C₆H₄OMe; R¹ = alkyl, aryl, ferrocenyl (Fc), thiophenyl, CO₂Me or SiMe₃; R² = H, Me or CO₂Me) were synthesized in moderate to high yields from the thermal decarbonylation of the bis-carbonyl precursors **2a–o**, and were structurally characterized by IR and NMR spectroscopy, and single crystal X-ray diffraction in four cases. Electrochemical behavior of one complex was also investigated. Complexes **3a–o** comprise a highly functionalized, multisite amino-(cyano)allylidene ligand, including metal coordination of a tertiary amine group. Selected complexes displayed negligible to moderate catalytic activity in CO₂/propylene oxide coupling, working under ambient conditions. Additionally, they were

investigated as catalysts for the conversion of benzaldehyde to the corresponding borate ester **6a**, using pinacolborane (HBpin) as the borylating agent. Most complexes achieved good conversions at room temperature with 1% catalyst loading, and data highlight the significant influence of the multisite ligand substituents on the catalytic performance. Notably, complex **3m** (featuring R = 4-methoxyphenyl, R¹ = Fc, R² = H) displayed the highest activity and effectively catalyzed the hydroboration of various aldehydes and ketones. A plausible mechanistic cycle involves metal coordination of the carbonyl substrate, its activation being possibly facilitated by intramolecular interactions.

Introduction

Transition metal complexes hold significant potential in homogeneous catalysis, with the design of suitable organometallic structures being crucial to the development of efficient catalytic systems, where the metal centre(s) and the ligands can play complementary roles during synthetic transformations.^[1,2] In the pursuit of sustainability, iron complexes have gained particular attention due to iron abundance in the earth's crust, relative nontoxicity in many forms, and versatile chemistry associated with a range of accessible oxidation states.^[3–5]

Turning to diiron complexes could represent an increasingly favourable approach. Indeed, it has been widely recognized that dinuclear metal complexes offer cooperative effects from the two interconnected metal centres, resulting in enhanced synthetic opportunities compared to homologous mononuclear species.^[6–10] Remarkably, [FeFe]-hydrogenase enzymes, responsible for bacterial dihydrogen production, feature an organometallic diiron core comprising cyanide and carbonyl ligands, highlighting the potential of these bimetallic units in catalysis.^[11] The easily available, cost-effective and easy-to-handle $[\text{Fe}_2\text{Cp}_2(\text{CO})_4]$ (Cp = $\eta^5\text{-C}_5\text{H}_5$) compound, serves as a benchmark starting material for obtaining a diverse array of diorganoiron structures.^[12–14] Essentially, the stepwise substitution of two carbonyl ligands allows for the construction of functionalized, multisite hydrocarbyl ligands under regioselective control. The complementary electronic properties of the two Cp (π -donor) and the residual CO (π -acceptor) ligands confer strong robustness to the resulting diiron complexes, with the iron(I) centres tightly bound to ligands. This coordinative saturation typically hampers the use of these complexes in catalysis, but exceptions are possible when two spatially close ligands can function as catalytic sites.^[15,16]

Among the derivatives of $[\text{Fe}_2\text{Cp}_2(\text{CO})_4]$ accessible through the sequential CO-removal approach, vinyliminium complexes (**1**) can be obtained via a straightforward reaction sequence involving the uncommon regioselective coupling of isocyanide and alkyne units (Scheme 1, first step).^[17–22] The synthesis of **1** exhibits a remarkable broad scope, with over 150 compounds reported so far, and can be scalable to gram/multigram

[a] C. Zappelli,[†] S. Schoch, G. Bresciani, T. Funaioli, F. Marchetti
Department of Chemistry and Industrial Chemistry, University of Pisa, Via G. Moruzzi 13, I-56124 Pisa
E-mail: fabio.marchetti@unipi.it

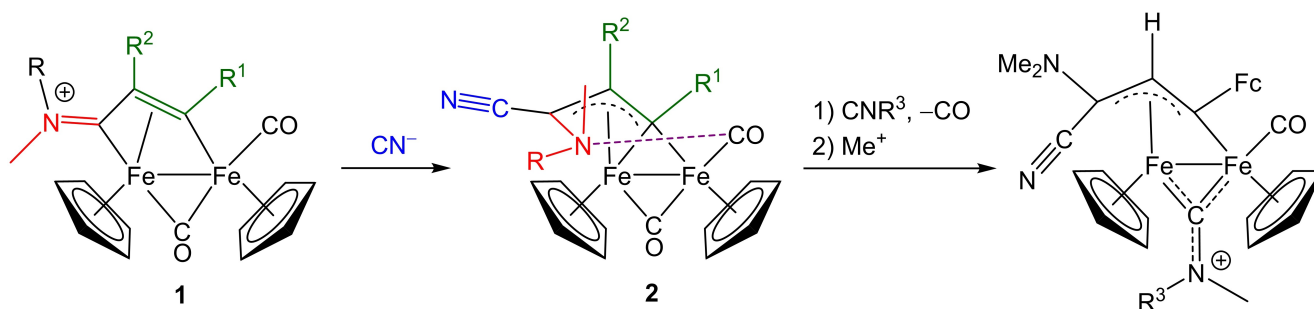
[b] F. Taglieri,[†] A. Di Giuseppe, M. Crucianelli
Department of Physical and Chemical Sciences, University of L'Aquila, Via Vetoio snc, I-67100 L'Aquila
E-mail: andrea.digiuseppe@univaq.it
marcello.crucianelli@univaq.it

[c] S. Zacchini
Department of Industrial Chemistry "Toso Montanari", University of Bologna, Via P. Gobetti 85, I-40129 Bologna

[†] These authors contributed equally to the work.

Supporting information for this article is available on the WWW under <https://doi.org/10.1002/cctc.202400811>

© 2024 The Author(s). ChemCatChem published by Wiley-VCH GmbH. This is an open access article under the terms of the Creative Commons Attribution License, which permits use, distribution and reproduction in any medium, provided the original work is properly cited.



Scheme 1. Diiron vinyliminium complexes (**1**) obtained by regioselective coupling of isocyanides (CNR, red) and alkynes ($R^1C\equiv CR^2$, green); cyanide addition (blue) affording amino-(cyano)allylidene complexes (**2**); subsequent CO substitution route leading to derivatives with an aminocarbonyl as additional bridging hydrocarbyl ligand. R = alkyl, aryl; R^1 = alkyl, aryl, thiophenyl, silyl, carboxylate et al.; R^2 = H, alkyl, carboxylate; Fc = ferrocenyl; R^3 = alkyl, naphthyl. Intramolecular amine-CO interaction is evidenced in **2**.

quantities, making them a versatile platform for exploring new organometallic reactivity patterns.

A simple method to further functionalize the vinyliminium moiety consists in cyanide addition, which is generally directed to the iminium carbon in a stereoselective fashion.^[23,24] In the resulting amino-(cyano)allylidene complexes (**2**), an intramolecular interaction between the amino-nitrogen lone pair and the terminal CO ligand places the cyano group in a syn orientation relative to the adjacent R^2 substituent (Scheme 1).^[25] Our interest in potential modifications of the structure of **2** prompted us to investigate the possibility of CO extrusion. In previous work, we reported that CO-isocyanide substitution in **2** provides access to rare Janus-type organometallic complexes, containing two bridging functionalized N-hydrocarbyl ligands (Scheme 1, second step).^[26]

The present study describes the thermal decarbonylation of **2**, resulting in a novel structural motif where the coordination vacancy generated by CO release is filled with a nitrogen atom (structure **3** in Scheme 2). We hypothesized that the tertiary amine nature of this function, combined with a proper choice of ligand substituents, might favour coordination flexibility, thereby facilitating catalytic transformations. Our primary focus was on the hydroboration of aldehydes and ketones to produce organoborate esters, valuable intermediates in organic synthesis.^[27–29] Traditionally, hydroboration relies on Lewis acidic boron reagents like $BH_3\cdot THF$, but their high reactivity and sensitivity to moisture make them difficult to handle. A significant advancement in this field is transition metal-catalysed hydroboration, employing safer reducing agents like pinacolborane (HBpin) or catecholborane (HBcat). This approach has led to development of a diverse array of organometallic catalysts,^[30] spanning from precious metals (e.g., rhodium,^[31] iridium,^[32] ruthenium,^[33] and rhenium^[34]) to s-block metals,^[35] rare-earth metal,^[36] and 3d-transition metals (e.g., manganese,^[37] cobalt,^[38] copper,^[39] and zinc^[40]). Recently, various iron complexes have gained attention as attractive candidates for catalysing hydroboration reactions. In 2017, Findaleter reported the first catalytic system based on iron, specifically iron(III) tris-acetylacetonate, which demonstrated efficient performance at room temperature.^[41] Subsequently, other iron compounds have been evaluated, showing a promising activity.

These include iron(II) complexes with various ligands,^[42–46] an iron(II) coordination polymer,^[47] iron(III)-SALEN adducts,^[48] and Fe_2O_3 -nanoparticles.^[49] However, the investigation of low-valent iron complexes, as well as diiron species,^[50,51] has been limited.^[52,53] In this context, the newly synthesized complexes **3** were tested as catalysts in hydroboration reactions with pinacolborane (HBpin).

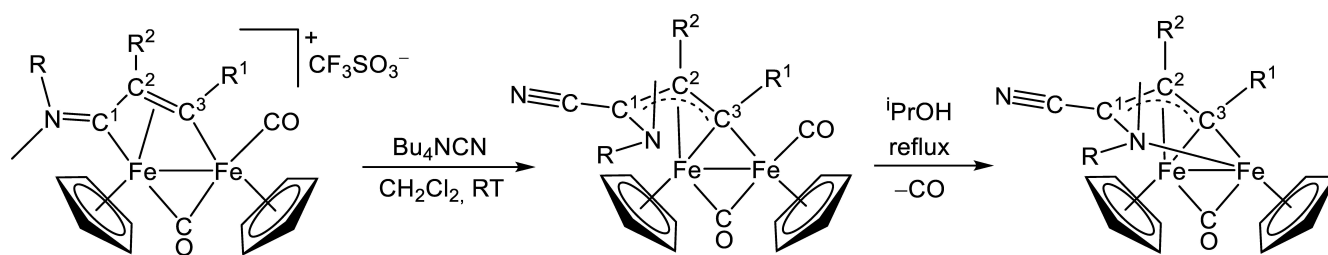
Results and Discussion

1) Synthesis and Crystallographic Characterization of Diiron Mono-Carbonyl Complexes

The bis-carbonyl complexes **2a–o** were synthesized from the respective vinyliminium precursors, **1a–o**, following the literature procedure involving tetrabutylammonium cyanide as CN^- source.^[23–25] Compounds **2d, h, i** are unprecedented and their full characterization is provided in the Experimental section. Since **1h** is obtained as a mixture of two inseparable regioisomers (**1h1** and **1h2**),^[19] the subsequent cyanide addition reaction yielded the corresponding products **2h1** and **2h2**, which were subsequently separated through careful column chromatography.

During our previous experiments assessing the aqueous stability of the cytotoxic complex **2a**,^[17] we noticed a slight conversion at 37 °C into a mono-carbonyl derivative. Investigating different solvents and reaction conditions, we identified refluxing isopropanol as the optimal medium to perform the decarbonylation process. This reaction was applied to a total of 15 cases, resulting in the selective formation of the novel diiron (Fe^I/Fe^I) complexes **3a–o** (Scheme 2). Purified by alumina chromatography, the complexes were isolated as air-stable solids in yields ranging from 44% to 97% (average yield: 75%). Interestingly, complex **2h2**, which comprises one CO_2Me substituent on C^2 carbon of the bridging C_3 chain, resulted inactive towards decarbonylation. In contrast, its isomer **2h1** and the analogous bis-substituted complex **2k** readily underwent conversion to the respective products **3h** and **3k**.

The crystal structures of **3a**, **3j**, **3k** and **3l** were elucidated by X-ray diffraction studies (Figure 1, Table 1). The discussion on



	R	R ¹	R ²		
1a	Me	Fc	H	2a	3a
1b	Me	Ph	H	2b	3b
1c	Me	3-C ₆ H ₄ OH	H	2c	3c
1d	Me	2-C ₆ H ₄ NH ₂	H	2d	3d
1e	Me	3-thiophenyl	H	2e	3e
1f	Me	Me	H	2f	3f
1g	Me	SiMe ₃	H	2g	3g
1h1	Me	CO ₂ Me	H	2h1	3h
1h2	Me	H	CO ₂ Me	2h2	No reaction
1i	Me	(CH ₂) ₃ C≡CH	H	2i	3i
1j	Me	Me	Me	2j	3j
1k	Me	CO ₂ Me	CO ₂ Me	2k	3k
1l	Cy	Fc	H	2l	3l
1m	4-C ₆ H ₄ OMe	Fc	H	2m	3m
1n	CH ₂ CH=CH	Fc	H	2n	3n
1o	CH ₂ Ph	Fc	H	2o	3o

Scheme 2. Decarbonylation reaction (synthesis of **3**) of amino-(cyano)allylidene diiron complexes (**2**), obtained from cyanide addition to vinyliminium precursors (**1**). Fc = (η⁵-C₅H₄)FeCp (ferrocenyl); thiophenyl = C₄H₃S; Cy = C₆H₁₁ (cyclohexyl).

bonding parameters focuses on complexes **3j**, **3k** and **3l**, since crystals of **3a** are racemically twinned. Indeed, even though the overall connectivity and geometry of **3a** compare well to **3j**, **3k** and **3l**, the use of restraints during its refinement makes bonding parameters less reliable. Compounds **3** originate from parent complexes **2** after formal elimination of a terminal CO, followed by its intra-molecular substitution by an amino group. The final products retain the *cis*-Fe₂Cp₂(μ-CO) core of **2** and the bridging amino-(cyano)allylidene ligand of **3j**, **3k** and **3l** display bonding parameters very similar to **2**. Both C(1)–C(2) [1.4508(19), 1.440(3) and 1.437(3) Å for **3j**, **3k** and **3l**, respectively] and C(2)–C(3) [1.4168(19), 1.421(3) and 1.401(3) Å] contacts show some π-character, and Fe(1)–C(1) [2.0417(14), 2.0432(18) and 2.034(2) Å], Fe(1)–C(2) [2.0263(14), 2.0031(18) and 2.015(2) Å], and Fe(1)–C(3) [2.0334(14), 2.0131(18) and 2.040(2) Å] distances are similar, in accord to η³ coordination of the allylidene group. The Fe(2)–C(3) distance [1.9359(14), 1.9239(18) and 1.950(2) Å] is an almost pure Fe–C σ-bond, as found in **2a** [1.964(3) Å] and **2j** [1.975(2) Å].^[17,24] The C(1)–N(1) distance [1.4893(18), 1.495(2) and 1.479(3) Å] is essentially a single bond and is slightly elongated compared to **2a**

[1.447(4) Å] and **2j** [1.437(2) Å], consistent with the coordination of N(1) to Fe(2). The Fe(2)–N(1) contact [2.0556(12), 2.0533(16) and 2.131(2) Å for **3j**, **3k** and **3l**, respectively] is very close to those found in other iron cyclopentadienyl complexes with a pendant tertiary amine group.^[54–56] The Fe(2)–N(1) bond may be described as a σ-bond, in line with the sp³ hybridization of N(1) [sum angles 329.6(19), 329.3(2) and 332.2(3)^o for **3j**, **3k** and **3l**, respectively]. The major consequence of replacing a terminal CO with an amine in going from **2** to **3** is the inversion of the asymmetry of the μ-CO ligand. Indeed, in the cases of **3j**, **3k** and **3l**, Fe(1)–C(11) [1.9578(14), 1.9952(19) and 1.957(3) Å] is longer than Fe(2)–C(11) [1.8686(14), 1.8714(19) and 1.871(3) Å], whereas for **2a** and **2j** Fe(1)–C(11) [1.911(3) and 1.914(2) Å] is slightly shorter than Fe(2)–C(11) [1.922(3) and 1.927(2) Å]. This is in keeping with the fact that the amino group bonded to Fe(2) in **3j**, **3k** and **3l** is a pure σ-donor, whereas the CO ligand bonded to Fe(2) in **2a** and **2j** is a substantial π-acceptor. The observed Fe(1)–C(11) and Fe(2)–C(11) distances of **2a**, **2j**, **3j**, **3k** and **3l** suggest, also, that the η³-allylidene bonded to Fe(1) is somehow intermediate between CO and an amine concerning its σ-donor/π-acceptor character.^[57,58]

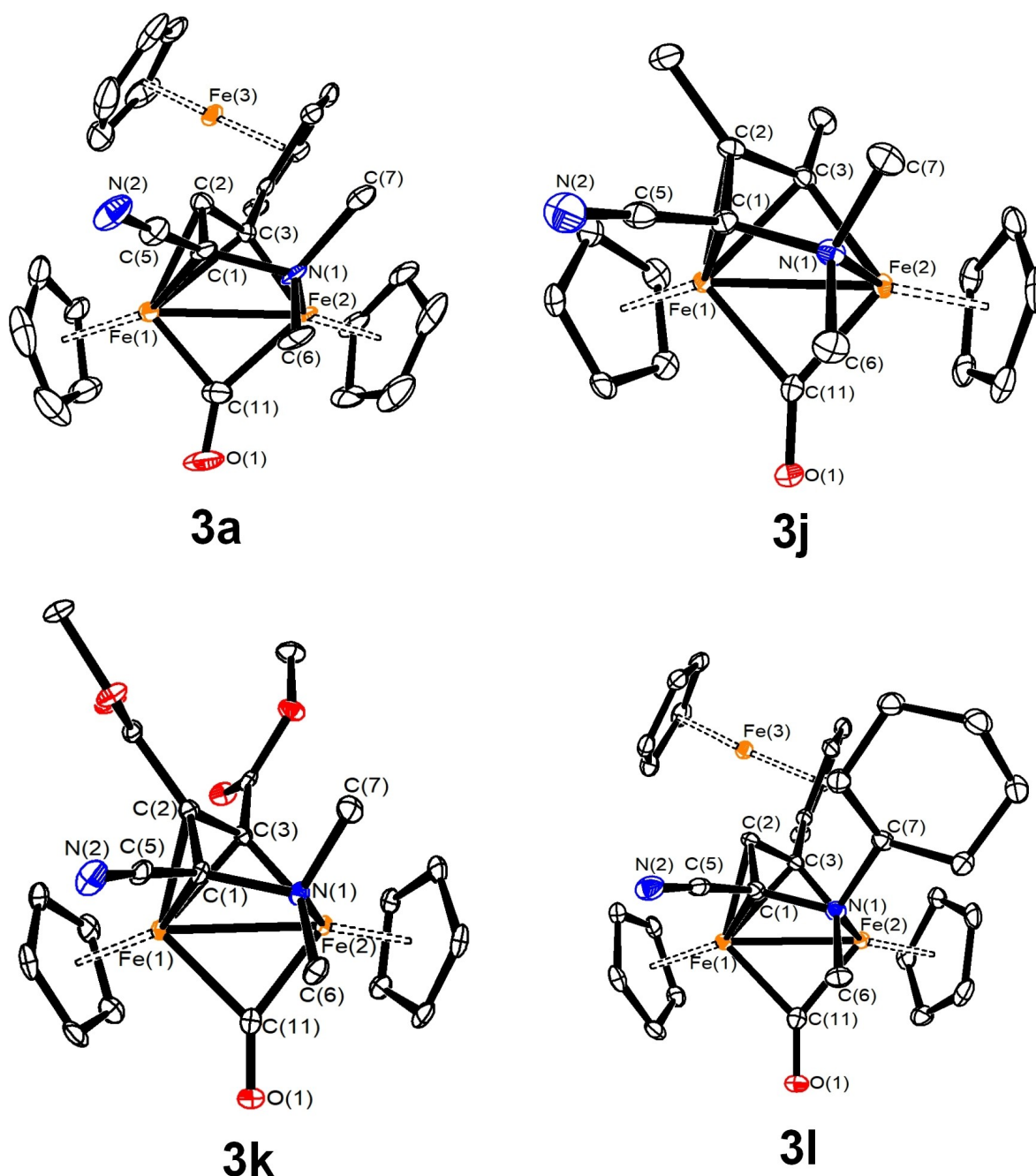


Figure 1. Views of the structures of **3a**, **3j**, **3k** and **3l** with key atoms labelled. Displacement ellipsoids are at the 50% probability level. Hydrogen atoms have been omitted for clarity.

The synthesis of the diiron complex **3d** (59% yield) proceeded with the side formation of the mono-iron(II) complex **4** (59% yield). This is attributable to the -NH_2 group, favouring the well-known fragmentation reaction of diiron vinyliminium complexes to mononuclear iron(II) species, cyclopentadiene and iron(0).^[59] The structure of **4** was confirmed by single crystal X-ray diffraction (Figure S1 in the Supporting Information). Complex **4** may be described as a 1-metalla-2-aminocyclopenta-1,3-dien-5-one complex, the bonding parameters related to the metallacycle resembling those reported for analogous compounds.^[18,20]

2) Spectroscopic Characterization and Spectroelectrochemistry

The IR spectra of **3a–o** (in dichloromethane solution) exhibit a common pattern with one band assigned to the bridging carbonyl ligand ($1735\text{--}1774\text{ cm}^{-1}$) and another band attributed to the triple carbon-nitrogen bond ($2192\text{--}2202\text{ cm}^{-1}$). The position of the former band is finely influenced by the electronic properties of the allylidene substituents, notably affecting the degree of $\text{Fe}\rightarrow\text{CO}$ backdonation. Remarkably, the highest value (1774 cm^{-1}) within the series is observed for **3k**,

Table 1. Main bond distances (Å) and angles (°) for **3a**, **3j**, **3k**, **3l** compared to literature data available for **2a**^[17] and **2j**^[24]

	3a	3j	3k	3l	2a	2j
Fe(1)–Fe(2)	2.5502(12)	2.5147(3)	2.5345(4)	2.5284(5)	2.5379(6)	2.5327(3)
Fe(1)–Cp _{av}	2.217(13)	2.089(3)	2.089(4)	2.092(7)	2.096(7)	2.102(8)
Fe(2)–Cp _{av}	2.058(11)	2.094(3)	2.098(4)	2.110(7)	2.122(7)	2.114(8)
Fe(1)–C(11)	1.749(7)	1.9578(14)	1.9952(19)	1.957(3)	1.911(3)	1.914(2)
Fe(2)–C(11)	1.927(6)	1.8686(14)	1.8714(19)	1.871(3)	1.922(3)	1.927(2)
Fe(1)–C(3)	2.112(6)	2.0334(14)	2.0131(18)	2.040(2)	2.025(3)	2.027(2)
Fe(2)–C(3)	1.725(6)	1.9359(14)	1.9239(18)	1.950(2)	1.964(3)	1.975(2)
Fe(1)–C(1)	2.289(7)	2.0417(14)	2.0432(18)	2.034(2)	2.071(3)	2.059(2)
Fe(1)–C(2)	2.096(6)	2.0263(14)	2.0031(18)	2.015(2)	2.025(3)	2.037(2)
Fe(2)–N(1)	2.169(5)	2.0556(12)	2.0533(16)	2.131(2)	–	–
C(11)–O(1)	1.124(8)	1.1846(18)	1.179(2)	1.184(3)	1.178(4)	1.173(2)
C(1)–C(2)	1.361(8)	1.4508(19)	1.440(3)	1.437(3)	1.446(4)	1.469(2)
C(2)–C(3)	1.411(8)	1.4168(19)	1.421(3)	1.401(3)	1.414(4)	1.418(2)
C(1)–N(1)	1.461(8)	1.4893(18)	1.495(2)	1.479(3)	1.447(4)	1.437(2)
C(1)–C(5)	1.461(8)	1.441(2)	1.445(3)	1.440(4)	1.467(5)	1.467(2)
C(5)–N(2)	1.164(9)	1.149(2)	1.147(3)	1.145(3)	1.145(4)	1.143(2)
Fe(1)–C(11)–Fe(2)	87.7(3)	82.14(6)	81.84(8)	82.64(10)	82.94(13)	82.49(6)
Fe(1)–C(3)–Fe(2)	82.7(2)	78.58(5)	80.11(7)	78.61(9)	79.01(11)	78.51(5)
C(1)–C(2)–C(3)	117.6(6)	109.36(12)	109.80(16)	111.3(2)	123.6(3)	119.2(2)
C(1)–C(5)–N(2)	178.7(7)	177.74(16)	176.0(2)	176.4(3)	179.3(4)	175.2(2)
C(1)–N(1)–C(6)	107.1(5)	109.52(11)	111.66(14)	109.86(19)	113.2(3)	114.21(13)
C(1)–N(1)–C(7)	117.8(5)	112.46(11)	109.70(14)	111.37(18)	111.3(3)	111.26(14)
C(6)–N(1)–C(7)	103.2(5)	107.62(11)	107.97(14)	110.93(19)	109.9(3)	110.20(14)
C(1)–N(1)–Fe(2)	90.7(3)	97.00(8)	97.93(10)	95.31(14)	–	–

featuring two electron-withdrawing methylcarboxylato groups, whereas the lowest value (1735 cm⁻¹) is found for **3i**, containing a donating pent-4-yn moiety. The CO wavenumber is also influenced by the amino substituents, albeit to a lesser extent.

The NMR spectra of **3a–k** (in CDCl₃), featuring two methyl groups on the amine, display a single set of resonances. However, these methyls are non-equivalent, due to the nitrogen atom being bonded to the iron. For instance, they resonate at 2.25 and 1.44 ppm (¹H) and 57.0 and 50.9 ppm (¹³C) in the case of **3d**. These ¹³C NMR signals are significantly deshielded compared to the bis-carbonyl precursor **2d** (49.5, 49.2 ppm). Compounds **3m–o**, with two distinct N-substituents, exist in CDCl₃ solution as pairs of stereoisomers. On the other hand, only one stereoisomer was observed for **3l**, presumably driven by the steric hindrance of the cyclohexyl group. The ¹H NMR spectra of complexes with R²=H reveal the significant alkenic character of this hydrogen, resonating in the range of 6.46 to 5.80 ppm. The ¹³C NMR data for C¹, C² and C³ carbons closely resemble those related to the precursors **2**, confirming that the amino-(cyano)allylidene ligand is minimally affected by the loss of one CO ligand. The low-field chemical shift of C³ reveals the allylidene character of this bridging carbon,^[60,61] and is correlated with the electronic features of the R¹ substituent. For instance, it falls at 177.8 ppm in **3k** (R¹=CO₂Me) and at 194.6 ppm in **3i** [R¹=(CH₂)₃C≡CH]. A comparative view of the

salient spectroscopic data of **3a–o**, and their selected precursors **2**, is supplied in the Supporting Information (Table S1).

As representative of the **3a–o** series, complex **3n** underwent additional characterization by electrochemical techniques. The electrochemical and spectroelectrochemical behaviour of **3n** was investigated at a platinum working electrode at room temperature, in CH₂Cl₂ solutions containing [NBu₄]PF₆ 0.2 M as the supporting electrolyte. The voltammetric profile between –2.0 and +1.0 V is characterized by two consecutive one-electron oxidation processes (Figure S42) at the formal electrode potentials of +0.21 V and +0.64 V (vs Ag/AgCl), respectively. Both processes exhibit electrochemical and chemical reversibility. The *in situ* IR spectroelectrochemical investigation of a CH₂Cl₂/[NBu₄]PF₆ solution of **3n** in an optically transparent thin-layer electrochemical (OTTLE) cell^[62] proved the chemical stability of the two oxidized species even in the longer timescale of the spectroelectrochemistry.

As the potential of the working electrode was gradually increased from 0.0 to +0.96 V (at a scan rate of 1 mV s⁻¹), two successive upshifts of the two IR bands corresponding to the CN and bridging-CO stretching of **3n** (respectively at 2195 and 1747 cm⁻¹) were observed (Figure 2). In the potential range between 0.0 and +0.6 V, the first electron removal moved the bands up to 2214 and 1830 cm⁻¹, while, when the potential was further increased up to +0.96 V, the absorptions were shifted

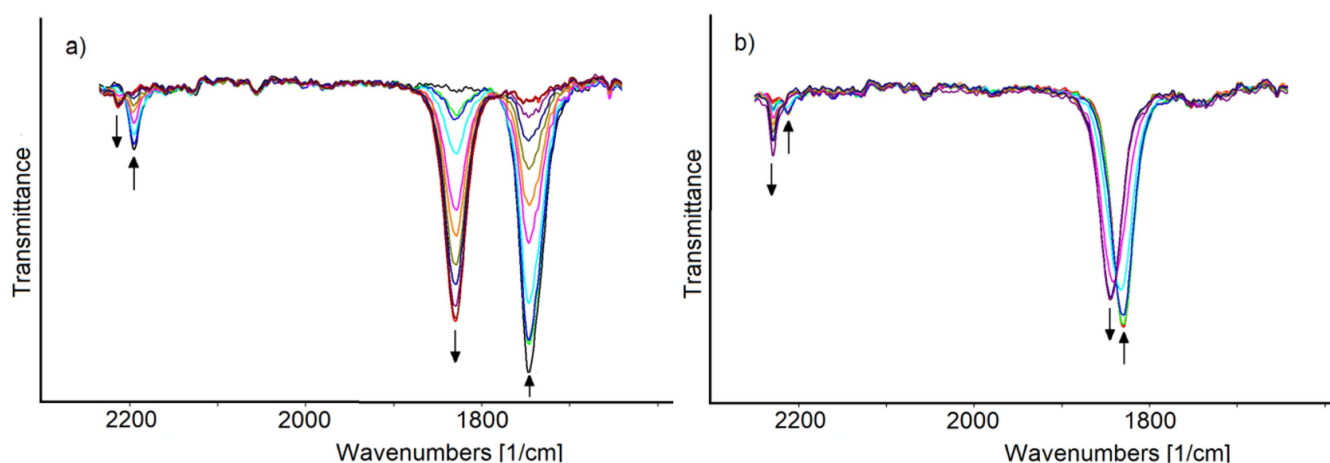


Figure 2. IR spectral changes of a CH_2Cl_2 solution of **3n** recorded in an OTLE cell during the progressive increase of the potential a) from 0.0 to +0.6 V (vs. Ag pseudoreference electrode); b) from +0.6 to +0.96 V (vs. Ag pseudoreference electrode). Scan rate 1.0 mV s^{-1} , spectra collected every minute. $[\text{NBu}_4]\text{PF}_6$ (0.2 mol dm^{-3}) as the supporting electrolyte. The absorptions of the solvent and supporting electrolyte have been subtracted.

to 2230 and 1845 cm^{-1} . In the backward reduction, the initial spectrum was completely restored, pointing out the high stability of the oxidation products $[\text{3n}]^+$ and $[\text{3n}]^{2+}$. This behaviour can be compared to that of **2a**,^[17] bearing an additional CO ligand, for which two oxidative processes were recognized at higher potentials and followed by relatively fast decomposition reactions. Furthermore, we observed that the shift of the ν_{CO} following the first oxidation (83 cm^{-1}) is greater than that of the second one (15 cm^{-1}), suggesting the removal of the first electron centred at $[\text{Fe}^{\text{I}}\text{Fe}^{\text{I}}]$ core and the second one at the ferrocenyl moiety.

3) Catalytic Activity of new Diiron Complexes

As an initial exploration of the catalytic properties of the newly synthesized class of complexes **3**, we conducted tests to evaluate their ability to catalyse the coupling of carbon dioxide with propylene oxide to produce propylene carbonate. These experiments were carried out at room temperature and ambient CO_2 pressure, using tetrabutylammonium bromide as a co-catalyst. Details of these experiments can be found in the Supporting Information. Developing efficient catalytic systems for CO_2 activation into cyclic carbonates is a highly active research area, particularly those employing earth-abundant metals and mild reaction conditions.^[63–66] While most of the synthesized complexes displayed minimal catalytic activity, complexes **3d** and **3m** exhibited modest to moderate activity. This suggests that the catalytic performance of complexes **3** can be influenced by the steric and electronic properties of the substituents on the amino(cyano)allylidene ligand. Notably, the presence of specific functional groups, such as the aniline group in **3d** and the ferrocenyl moiety in **3m**, might contribute to enhanced activity.

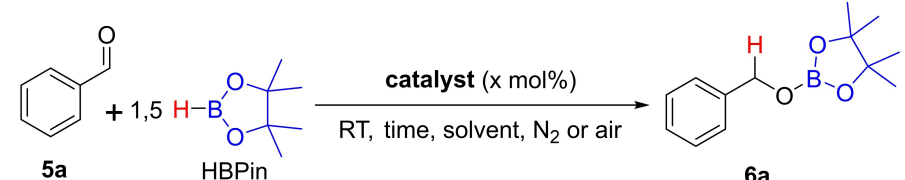
To further explore the catalytic potential of complexes **3**, we investigated their activity in the hydroboration of carbonyl compounds. The reaction between with benzaldehyde (**5a**) and

pinacolborane (HBPin) at room temperature was chosen as a model system, and the reactions were monitored and quantified using GC-FID (Table 2). We started evaluating the activity of complexes **3a**, **3b** and **3g**, which quite well cover the chemical space of the functionalities on the amino-(cyano)allylidene ligand.

Dry THF was chosen as the initial solvent due to the higher solubility of most catalysts. Control reaction without any catalyst yielded only 11% of conversion after 6 hours (entry 1). In a preliminary experiment performed using 2 mol% of **3a**, **3b** and **3g** as catalysts, in the presence of 1.5 eq. of HBPin, at room temperature under air, we observed conversions of 80, 78 and 44%, respectively, after 6 h (entries 2–4). $^1\text{H-NMR}$ analysis of the reaction mixtures confirmed complete selectivity, with only the starting material (**5a**) and the desired product, 2-(benzyloxy)-4,4,5,5-tetramethyl-1,3,2-dioxaborolane (**6a**), being detected. Exclusion of air from the catalytic system significantly improved the performances of the three $[\text{FeFe}]$ complexes, leading to nearly complete conversion within six hours (entries 5–7). Interestingly, Zhang and coworkers reported that the Fe^{II} -coordination polymer used as pre-catalyst exhibited limited activity under N_2 atmosphere, while exposure to air enhanced the activity, presumably due to oxidation to Fe^{III} .^[47]

In our case, the significantly higher conversion observed under an inert atmosphere (entries 2–4 vs. 5–7) strongly suggests that feasible air-oxidation of the $[\text{Fe}^{\text{I}}\text{Fe}^{\text{I}}]$ complexes **3** might be detrimental to their catalytic activity, despite the relative stability of the oxidation products (vide infra). Reducing the reaction time from 6 to 3 hours (entries 8–10) had minimal impact on the percentage of converted substrate, making it difficult to differentiate between the catalytic performances of the various catalysts. Subsequently, the reactions were repeated with reduced catalyst loading, from 2 mol% to 1 mol% (entries 11–13). This revealed a clearer distinction between the activities of the three complexes, with **3a** achieving nearly complete conversion in 6 hours (entry 14). We then investigated the influence of the solvent on the catalytic reaction. The

Table 2. Optimization of the hydroboration of benzaldehyde with HBPIn mediated by **3(a,b,g)**.^[a]



Entry	catalyst	t (h)	cat. (mol %)	N ₂	solvent	Conv. (%) ^[b]
1	–	6	–	x	THF	11
2	3a	6	2	x	THF	80
3	3b	6	2	x	THF	78
4	3g	6	2	x	THF	44
5	3a	6	2		THF	96
6	3b	6	2		THF	96
7	3g	6	2		THF	86
8	3a	3	2		THF	89
9	3b	3	2		THF	84
10	3g	3	2		THF	74
11	3a	3	1		THF	82
12	3b	3	1		THF	68
13	3g	3	1		THF	31
14	3a	6	1		THF	96
15 ^[d]	3a	24	2		C ₆ D ₆	33
16 ^[d]	3a	24	2		CDCl ₃	20
17	3a	24	2		CH ₃ CN	n.d.

[a] Reaction conditions: 0.25 mmol of **5a**, 1.5 equiv. of HBPIn, 0.5 mL of dry THF, selected molar percentage of diiron catalyst. [b] Conversion based on the consumption of benzaldehyde, determined by GC-FID using *n*-dodecane as the internal standard. Selectivity to **6a** determined by NMR using 1,3,5-trimethoxybenzene as the internal standard. In all cases, **6a** was the only observed reaction product. [d] Reaction performed in NMR tube and monitored by ¹H-NMR using 1,3,5-trimethoxybenzene as the internal standard.

reaction was carried out in NMR tubes using either C₆D₆ or CDCl₃ as the solvent and 2 mol% of **3a**. However, negligible conversion was observed in both cases (entries 15 and 16). When acetonitrile was employed as the solvent, no conversion was observed, possibly due to deactivation of the catalyst caused by solvent coordination (entry 17).^[51]

We then compared the catalytic performance of a selection of complexes, namely **3a–d**, **3g**, **3l–m** and **3o**, in the benchmark reaction with [benzaldehyde]=0.5 M in THF, 1.5 eq. of HBPIn, and 1 mol% of catalyst, at room temperature (see Table 3). This selection of complexes can be divided into two structural sub-families: the first family (**3a**, **3b**, **3c**, **3d**, **3g**) features a small tertiary amine (NMe₂, R=Me in Scheme 2) and a varying R¹ substituent. The second family (**3l**, **3m**, **3o**) features a bulky substituent on the tertiary amine (R≠Me) alongside the ferrocenyl (Fc) moiety. Data in Table 3 show significant variability in catalyst activity, likely due to the different stereo-electronic environments experienced by the iron centres. We were pleased to observe that all complexes exhibited notable reactivity even after three hours. However, a clearer differentiation in their performances is evident at a one-hour reaction time. When comparing the catalytic activity of

complexes with varying R¹ substituents (entries 1–3), we notice that **3a** (R¹=Fc) outperforms **3b** (R¹=Ph). Complex **3g**, featuring R¹=SiMe₃, demonstrates the lowest activity in this series. The distinct R¹ groups are directly connected to the bridging carbene C³, tuning its electronic properties (as showed by IR and NMR spectroscopic data, see above) and, consequently, influencing the activity of the diiron frame. Introducing a functional group onto the phenyl ring of the R¹ substituent significantly impacts catalytic activity (entry 2 vs entries 4–5). Specifically, the presence of a *m*-OH (**3c**) or a *o*-NH₂ (**3d**) group leads to a complete conversion in 3 hours, with **3d** being more active than its congener **3c**, converting 88% of benzaldehyde to **6a** in 1 h (entry 5 vs 7). In principle, these moieties could form hydrogen bonds with polar substrates, like carbonyl compounds, facilitating their approach to the catalytically active metal centre. To investigate the role of the proximity of the amino group on the phenyl substituent to the bimetallic core, a control experiment was conducted. The reaction with complex **3b** was repeated with 1 equivalent of free aniline (**3b**/aniline molar ratio=1) to mimic the presence of the *o*-NH₂ unit in **3d**. Interestingly, this addition resulted in a decrease in substrate conversion, highlighting the importance of the designed

Table 3. Comparison of the catalytic properties of [FeFe] complexes in the hydroboration of benzaldehyde with HBPin.^[a]

Entry	[FeFe]	t (h)	Conv. (%) ^[b]
1	3a	3	82
2	3b	3	68
3	3g	3	31
4	3c	3	> 99
5	3c	1	74
6	3d	3	> 99
7	3d	1	88
8 ^[c]	3b + 1 eq. aniline	3	28
9 ^[d]	3d	3	19
10	3l	3	90
11	3l	1	49
12	3m	3	> 99
13	3m	1	96
14 ^[d]	3m	3	30
15	3o	3	> 99
16	3o	1	67
17	Fe ₂ Cp ₂ (CO) ₄	3	62

[a] Reaction conditions: 0.25 mmol of **5a**, 1.5 equiv. of HBPin, 0.5 mL of dry THF, 1 mol% of diiron catalyst. [b] Conversion based on the consumption of benzaldehyde, determined by GC-FID using *n*-dodecane as the internal standard. Selectivity to **6a** determined by NMR using 1,3,5-trimethoxybenzene as the internal standard. In all cases, **6a** was the only observed reaction product. [c] Reaction performed with the addition of 2.5 μmol of aniline (1 eq. respect **3b**). [d] Reaction performed with 0.5 mol% of catalyst.

architecture of the catalyst for optimal activity (entry 8 vs. entries 2 and 6). Additionally, the stereo-electronic properties of the tertiary amine have a significant impact on the catalytic activity of the diiron complexes. More in detail, substituting a methyl (**3a**) with more sterically demanding groups such as cyclohexyl (**3l**), 4-methoxyphenyl (**3m**) or benzyl (**3o**) increases the conversion from 82% to 90% for **3l** and to completeness in the other cases (entry 1 vs entries 10, 12 and 15, respectively). These data can be rationalized in terms of the stereo-electronic

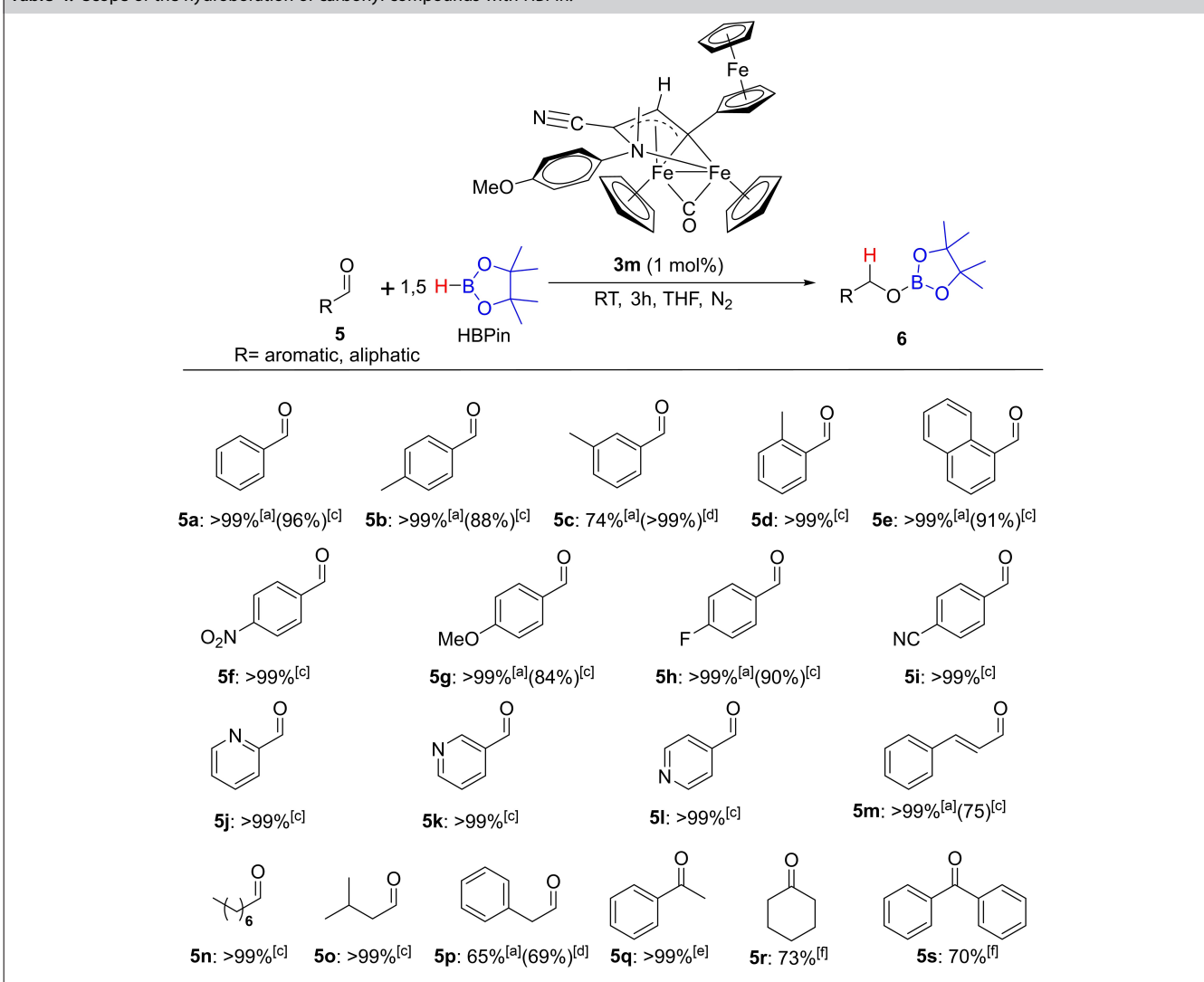
features of the tertiary amine: the conjugation with the 4-methoxyphenyl residue and the greater rigidity of this pendant group, compared to benzyl for **3o** and cyclohexyl for **3l**, likely weakens the coordination of nitrogen to iron. The weakened coordination of this fragment of the multisite amino-(cyano)allylidene ligand might favour the bonding of the substrate to the iron centre, thereby increasing the activity of the catalyst. For comparison, the commercial available diiron(II) precursor [Fe₂Cp₂(CO)₄] was also tested as a catalyst. As shown

in entry 17, this compound revealed to be the least active (excluding **3g**), highlighting the crucial role of the versatile amino-(cyano)allylidene ligand in this catalysis. To further optimize reaction conditions, we lowered the catalytic load of the two most active complexes, **3d** and **3m**, to 0.5 mol% (entries 9 and 14). While this lowered amount resulted in insufficient conversion for both complexes, **3m** still displayed superior catalytic properties, emerging as the most effective catalyst in this study.

Encouraged by the promising results, especially regarding the high activity of **3m**, we further explored the substrate scope of the reaction with a series of carbonyl compounds exhibiting diverse stereo-electronic properties (Table 4). Gratifyingly, all tested substrates yielded the corresponding borate esters exclusively. Tolualdehydes (**5b–d**) were employed to evaluate the effect of steric hindrance of the substrate. Since the C=O

bond plays a crucial role in this reaction, a decrease in reactivity proportional to the proximity of the methyl substituent to the carbonyl group should be expected. Surprisingly, a different trend was observed. Thus, *ortho*-substituted **5d** underwent complete conversion within 1 hour, while *para*- (**5b**) and *meta*-substituted (**5c**) tolualdehydes required 3 and 6 hours, respectively. 1-Naphthaldehyde (**5e**) was included in this study, to further assess the influence of steric effects around the aromatic ring. The results confirm that the reactivity of **5e** is more in line with 2- and 4-tolualdehydes than with 3-substituted tolualdehyde, suggesting a well-defined spatial arrangement between the catalyst active site and the substrate. Then we examined the electronic effects of substituents on the aromatic ring. The presence of a strong electron-donating group as 4-methoxy (**5g**) slightly decreased the reactivity of the catalytic system (achieving 84% conversion after 1 h). Conversely, electron-

Table 4. Scope of the hydroboration of carbonyl compounds with HBPIn.^[a,b]

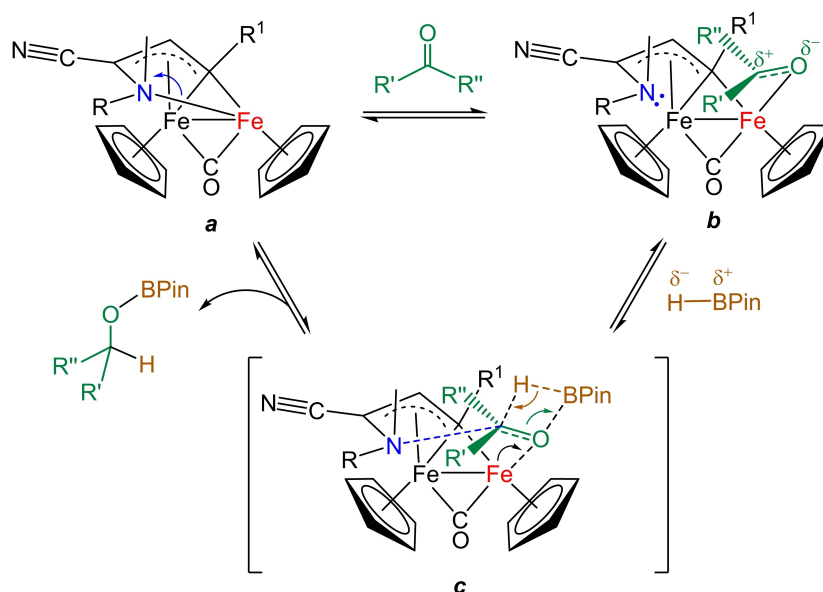


[a] Reaction conditions: 0.25 mmol of aldehyde, 1.5 equiv. of HBPIn, 0.5 mL of dry THF, 1 mol% of **3m** at RT for 3 h. [b] Conversion based on the consumption of aldehyde, determined by GC-FID using *n*-dodecane as the internal standard. Selectivity to borate ester was determined by NMR using 1,3,5-trimethoxybenzene as the internal standard. In all cases, the corresponding borate ester was the only observed reaction product. [c] Reaction time: 1 h. [d] Reaction performed at 50 °C for 6 h with 3 equiv. of HBPIn. [e] Reaction performed at 50 °C for 1 h. [f] Reaction performed at 50 °C for 3 h.

withdrawing groups like 4-NO₂ (**5f**) or 4-CN (**5i**) were well tolerated, resulting in complete conversion after 1 hour of reaction. This reactivity trend, observed in previous studies,^[47] reflects variations in electrophilicity of the carbonylic carbon. Notably, the two substrates containing potentially reducible groups (**5f** and **5i**) underwent hydroboration exclusively at the aldehyde moiety. Halogenated compounds like 4-fluorobenzaldehyde (**5h**) were also compatible with the catalytic system, achieving quantitative conversion to the corresponding borate ester in 3 hours without any formation of the hydrodehalogenated product. The presence of a coordinating group such as pyridine was also well tolerated, regardless of the nitrogen position. In fact, 2-, 3- and 4- pyridinecarboxaldehydes (**5j**, **5k** and **5l**, respectively) were completely converted in one hour, similar to other electron-poor aromatic aldehydes. The chemoselectivity of the catalytic system was further confirmed with *trans*-cinnamaldehyde (**5m**). This conjugated aldehyde is notoriously electrophilic on both α and γ carbons, but even in this case the reaction occurred selectively at the C=O bond, yielding complete conversion to the borate ester after 3 hours. Moving on to aliphatic aldehydes, both linear *n*-octanal (**5n**) and branched isovaleraldehyde (**5o**) were active substrates, reaching completion within 1 hour. Surprisingly, phenylacetaldehyde (**5p**) proved to be the most challenging aldehyde in this study. Even with elevated reaction temperature (50 °C) and excess borulating agent, it only achieved 69% conversion. In this case, keto-enol tautomerism likely favours the enolic form, hindering further reaction progress. To expand the scope of this catalytic system, we investigated a series of ketones. The lower reactivity of this class of compounds necessitated conducting the reactions at 50 °C. Gratifyingly, acetophenone (**5q**) reacted smoothly, providing the corresponding borate ester with full conversion in only 1 hour. However, a decrease in conversion was observed for more hindered substrates like cyclohexanone

(**5r**) and benzophenone (**5s**), presumably due to increased steric hindrance around the carbonyl group.

Based on the experimental observations, we propose a tentative mechanistic cycle for the hydroboration of carbonyl compounds catalysed by the diiron complexes **3** (see Scheme 3). Displacement of the amine from iron coordination, in the presence of large amounts of carbonyl substrate, would lead from complex **a** to complex **b**. As a matter of fact, data in Table 3 indicate that the activity of the diiron catalysts strongly depends on the amine substituent R, with the *p*-methoxyphenyl group providing the highest performance. It is reasonable to assume that this rigid and sterically hindered substituent influences the Fe–N interaction, shifting the equilibrium towards the formation of complex **b**. This hypothesis aligns with the recent work of Xiao, Zhong et al., where the coordination flexibility of one carbonyl ligand within a low valent diiron complex generated a vacant metal site initiating the hydroboration reaction.^[51] In the present case, it is presumable that iron-coordination of the carbonyl substrate enhances its reactivity towards hydroborane addition, possibly with the adjuvant contribution of the pendant amine moiety, leading to the borate ester. According to our experimental findings, the activation of the carbonyl group could be further facilitated by hydrogen bond formation with adjacent –NH₂ or –OH units on R¹. The final step includes restoration of the Fe–N bond releasing the organic product. An alternative mechanism including hydride transfer from pinacolborane to the metal centres should be ruled out, based on the fact that the representative complex **3b** revealed absence of reactivity towards an excess of NaBH₄ as potential hydride source^[67] in THF solution, even at 50 °C (see Experimental for details).



Scheme 3. Proposed mechanism for the hydroboration of aldehydes/ketones with pinacolborane (HBpin) catalysed by diiron complexes of type **3**, comprising a pendant amine donor.

Conclusions

The construction of new organometallic structures based on earth-abundant metals is crucial for developing new efficient catalysts for environmentally benign organic transformations. In this context, iron stands out as a particularly appealing candidate. Diiron complexes provide significant advantages arising from the cooperativity of the dimetallic core, enabling the synthesis of bridging functionalized ligands that may be not accessible in analogous mononuclear structures. Here, we describe the stepwise building of a functionalized, multisite N-decorated hydrocarbyl ligand bound to the robust Fe₂Cp₂ framework, showing that the final decarbonylation step results in iron coordination of a tertiary amine moiety. The highly regio- and stereo-selective control of this organometallic synthesis, along with its broad scope, provides a robust range of diiron(I) complexes for catalytic studies. We demonstrate the effectiveness of these complexes in the pinacolborane hydroboration of aldehydes and ketones, a valuable organic conversion for which effective dinuclear and/or low valent iron catalysts have rarely been reported. We further reveal the possibility of fine-tuning catalytic activity by varying the substituents on the amino(cyano)allylidene moiety. Groups with specific steric and electronic properties significantly influence catalyst performance. Furthermore, the incorporation of small units capable of hydrogen bonding may further enhance catalytic activity. Overall, our findings highlight the potential of functionalized di-organoiron compounds in homogenous catalysis and emphasize the importance of metal-metal cooperativity in designing suitable structures for optimal catalytic performances.

Experimental

1) Synthesis and Characterization of Iron Complexes

General details. Organic reactants (TCI Europe, Merck or Thermo Fisher) and [Fe₂Cp₂(CO)₄] (Strem) were commercial products of the highest purity available and used without further purifications. Compounds **1a**,^[17] **1b–c**,^[18] **1d**,^[20] **1e–f**,^[17] **1g–h**,^[19] **1i**,^[21] **1j–k**,^[18] **1l–o**,^[17] **2a**,^[17] **2b–c**,^[25] **2e–f**,^[25] **2g**,^[24] **2j**,^[24] **2k**,^[25] **2l–o**^[23] were prepared according to the respective literature procedures. Chromatography separations were carried out under N₂ atmosphere on columns of deactivated alumina (Merck, 4% w/w water), using wet solvents. Unless otherwise specified, reactions were conducted under N₂ atmosphere using anhydrous (dichloromethane) or deaerated (isopropanol) solvents. Dry solvents used for catalysis were purchased from ERBADry (Carlo Erba), transferred under inert atmosphere in flame-dried bottles with J-Young caps (Rotaflo® system) and then stored over 4 Å molecular sieves. Dichloromethane was dried with the solvent purification system mBraun MB SPS5. Infrared spectra of solutions were recorded on a Perkin Elmer Spectrum 100 FT-IR spectrometer with a CaF₂ liquid transmission cell (2300–1500 cm⁻¹ range). IR spectra were processed with Spectragryph software.^[68] All iron products are indefinitely air-stable in the solid state and were stored in air once isolated. NMR spectra were recorded at ambient temperature on Bruker Avance II DRX400 or JEOL YH JNM-ECZ400S instruments equipped with broadband probes. Chemical shifts (expressed in parts per million) are referenced to the residual solvent peaks^[69] (¹H, ¹³C) or to external

standards.^[70] NMR spectra were assigned with the assistance of ¹H–¹³C (*gs*-HSQC and *gs*-HMBC) correlation experiments.^[71] NMR signals due to secondary isomeric forms (where it has been possible to detect them) are italicized. Materials and apparatus for electrochemistry and IR spectroelectrochemistry have been described elsewhere.^[23] Under the present experimental conditions, the one-electron oxidation of ferrocene occurred at E° = +0.45 V vs Ag/AgCl, KCl sat. Elemental analyses were performed on a Vario MICRO cube instrument (Elementar). The course of catalytic reactions was followed by gas chromatography using an Agilent 7820 GC-FID system, equipped with a J&W HP-5 Intuvo GC fused silica column module (30 m, 0.32 mm, 0.25 μm), and with a flame ionization detector (FID). Quantification of reaction products was performed *via* Nuclear magnetic resonance analyses (¹H NMR spectra) using a Bruker Avance III 400 MHz spectrophotometer, analysing the reaction mixture including 1,3,5-trimethoxybenzene as the internal standard.

1.1) Synthesis and Characterization of **2d,h,i**

General procedure. A solution of the selected diiron vinyliminium complex (**1**) in CH₂Cl₂ (ca. 10 mL) was treated with Bu₄NCN (1.2 eq.). After stirring for 2 hours at room temperature, IR spectroscopy indicated the quantitative conversion of the precursor. Hence, the reaction solution was loaded on top of an alumina column, previously packed with petroleum ether. Hexane and hexane/diethyl ether mixtures were used to elute impurities. The fraction corresponding to the desired product was collected using the indicated eluent. Solvent evaporation afforded an oily residue, which was dissolved in CH₂Cl₂ (ca. 2 mL). Subsequent pentane addition (ca. 15 mL) afforded a brown air-stable powder, which was dried under vacuum.

[Fe₂Cp₂(CO)(μ-CO){μ-η¹:η³-C³(2-C₆H₄NH₂)C²HC¹(CN)NMe₂}], **2d** (Figure 3)

From **1d** (207 mg, 0.334 mmol). Chromatography: CH₂Cl₂. Brown solid. Yield 140 mg (84%). Anal. calcd. for C₂₄H₂₃Fe₂N₃O₂: C, 57.98; H, 4.66; N, 8.45. Found: C, 57.31; H, 4.70; N, 8.32. IR (CH₂Cl₂): $\tilde{\nu}$ /cm⁻¹ = 2184w-m (C≡N), 1956vs (CO), 1780s (μ-CO). ¹H NMR (CDCl₃): δ /ppm = 7.69, 7.16, 6.95, 6.85 (m, 4 H, C₆H₄); 4.74, 4.58 (s, 10 H, Cp); 4.52 (s, 1 H, C²H); 3.70 (s, 2 H, NH₂); 2.34, 1.80 (s, 6 H, NMe₂). ¹³C{¹H} NMR (CDCl₃): δ /ppm = 264.4 (μ-CO); 198.5 (C³); 144.9, 141.7 (*ipso*-C₆H₄); 213.7 (CO); 127.2, 126.9, 118.1, 115.8 (C₆H₄); 120.5 (C≡N); 89.6, 86.2 (Cp); 83.6 (C²); 64.3 (C¹); 49.5, 42.2 (NMe₂).

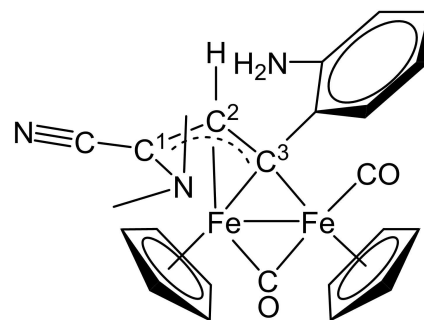


Figure 3. Structure of **2d**.

$[\text{Fe}_2\text{Cp}_2(\text{CO})(\mu\text{-CO})\{\mu\text{-}\eta^1\text{-}\eta^3\text{-C}^3(\text{CO}_2\text{Me})\text{C}^2\text{HC}^1(\text{CN})\text{NMe}_2\}],$ **2 h1**,
and $[\text{Fe}_2\text{Cp}_2(\text{CO})(\mu\text{-CO})\{\mu\text{-}\eta^1\text{-}\eta^3\text{-C}^3\text{HC}^2(\text{CO}_2\text{Me})\text{C}^1(\text{CN})\text{NMe}_2\}],$
2 h2 (Figure 4)

From **1 h** (308 mg, 0.525 mmol).

2 h1. Chromatography: THF/ CH_2Cl_2 (1:4 v/v). Dark-green solid. Yield 99 mg (41%). Anal. calcd. for $\text{C}_{20}\text{H}_{20}\text{Fe}_2\text{N}_2\text{O}_4$: C, 51.76; H, 4.34; N, 6.04. Found: C, 51.42; H, 4.30; N, 5.90. IR (CH_2Cl_2): $\tilde{\nu}/\text{cm}^{-1} = 2192\text{w}$ ($\text{C}\equiv\text{N}$), 1975vs (CO), 1798 s ($\mu\text{-CO}$), 1702 m (CO_2Me). ^1H NMR (CDCl_3): $\delta/\text{ppm} = 4.86$ (s, 1 H, C^2H); 4.81, 4.63 (s, 10 H, Cp); 4.06 (s, 3 H, CO_2Me); 2.23, 1.61 (s, 6 H, NMe_2). $^{13}\text{C}\{^1\text{H}\}$ NMR (CDCl_3): $\delta/\text{ppm} = 261.0$ ($\mu\text{-CO}$); 211.9 (CO); 181.2, 180.3 ($\text{CO}_2\text{Me} + \text{C}^3$); 120.5 ($\text{C}\equiv\text{N}$); 88.2, 86.7 (Cp); 81.0 (C^2); 63.6 (C^1); 52.5 (OMe); 49.3, 41.8 (NMe_2).

2 h2. Chromatography: CH_2Cl_2 . Brown solid. Yield 40 mg (17%). Anal. calcd. for $\text{C}_{20}\text{H}_{20}\text{Fe}_2\text{N}_2\text{O}_4$: C, 51.76; H, 4.34; N, 6.04. Found: C, 52.06; H, 4.26; N, 6.03. IR (CH_2Cl_2): $\tilde{\nu}/\text{cm}^{-1} = 2187\text{w}$ ($\text{C}\equiv\text{N}$), 1915vs (CO), 1796 s ($\mu\text{-CO}$), 1710 m (CO_2Me). ^1H NMR (CDCl_3): $\delta/\text{ppm} = 12.94$ (s, 1 H, C^3H); 4.95, 4.47 (s, 10 H, Cp); 3.89 (s, 3 H, CO_2Me); 2.09, 1.67 (s, 6 H, NMe_2). $^{13}\text{C}\{^1\text{H}\}$ NMR (CDCl_3): $\delta/\text{ppm} = 211.9$ (CO); 180.3 (C^3); 172.6 (CO_2Me); 119.6 ($\text{C}\equiv\text{N}$); 87.9, 86.6 (Cp); 86.1 (C^2); 59.0 (C^1); 52.9 (OMe); 47.8, 40.8 (NMe_2).

$[\text{Fe}_2\text{Cp}_2(\text{CO})(\mu\text{-CO})\{\mu\text{-}\eta^1\text{-}\eta^3\text{-C}^3(\text{CH}_2\text{CH}_2\text{CH}_2\text{CCH})\text{C}^2\text{HC}^1(\text{CN})\text{NMe}_2\}],$
2i (Figure 5)

From **1 i** (125 mg, 0.210 mmol). Chromatography: CH_2Cl_2 . Brown solid. Yield 83 mg (84%). Anal. calcd. for $\text{C}_{23}\text{H}_{24}\text{Fe}_2\text{N}_2\text{O}_2$: C, 58.51; H, 5.12; N, 5.93. Found: C, 58.72; H, 5.01; N, 6.08. IR (CH_2Cl_2): $\tilde{\nu}/\text{cm}^{-1} = 2254$ m ($\text{C}\equiv\text{C}$), 2189w ($\text{C}\equiv\text{N}$), 1968vs (CO), 1787 s ($\mu\text{-CO}$). ^1H NMR (CDCl_3): $\delta/\text{ppm} = 4.90, 4.46$ (s, 10 H, Cp); 4.39, 3.87 (m, 2 H, C^3CH_2); 4.36, (s, 1 H, C^2H); 2.60, 2.55 (m, 2 H, $\text{CH}_2\text{C}\equiv$); 2.37, 2.09 (m, 2 H,

$\text{CH}_2\text{CH}_2\text{CH}_2$); 2.28, 1.71 (s, 6 H, NMe_2); 2.15 (t, $^4J_{\text{HH}} = 2.6$ Hz, 1 H, $\text{C}\equiv\text{CH}$).

1.2) Synthesis and Characterization of **3 a–o**

General procedure. An isopropanol solution of the selected complex (**2**) was stirred at reflux under N_2 atmosphere for a variable time. Then volatiles were removed under vacuum, and the residue was dissolved in the minimum volume of CH_2Cl_2 or Et_2O . This solution was loaded on top of an alumina column, packed with petroleum ether. Hexane and hexane/diethyl ether mixtures were used to elute impurities. The fraction corresponding to the desired product was collected using the indicated eluent. Removal of the solvent under vacuum afforded a residue which was washed with pentane (ca. 20 mL). The resulting powdery solid was dried under vacuum.

$[\text{Fe}_2\text{Cp}_2(\mu\text{-CO})\{\mu\text{-k}^3\text{C,kN-C}^3(\text{Fc})\text{C}^2\text{HC}^1(\text{CN})\text{NMe}_2\}],$ **3 a** (Figure 6)

From **2 a** (234 mg, 0.397 mmol). Reaction time: 48 h. Chromatography: Et_2O . Dark-brown solid. Yield 167 mg (75%). Anal. calcd. for $\text{C}_{27}\text{H}_{26}\text{Fe}_3\text{N}_2\text{O}$: C, 57.70; H, 4.66; N, 4.98. Found: C, 57.45; H, 4.80; N, 5.04. IR (CH_2Cl_2): $\tilde{\nu}/\text{cm}^{-1} = 2196\text{w-m}$ ($\text{C}\equiv\text{N}$), 1747 s ($\mu\text{-CO}$). ^1H NMR (CDCl_3): $\delta/\text{ppm} = 6.23$ (s, 1 H, C^2H); 4.81, 4.55, 4.51, 3.99 (m, 4 H, C_5H_4); 4.51, 4.49 (s, 10 H, Cp); 3.99 (s, 5 H, Cp^{Fc}); 2.15, 1.41 (s, 6 H, NMe_2). $^{13}\text{C}\{^1\text{H}\}$ NMR (CDCl_3): $\delta/\text{ppm} = 284.0$ ($\mu\text{-CO}$); 184.8 (C^3); 119.7 ($\text{C}\equiv\text{N}$); 107.7 (*ipso*- C_5H_4); 83.9, 83.3 (Cp); 82.1 (C^2); 70.0, 68.3, 67.9, 67.5 (C_5H_4); 68.8 (Cp^{Fc}); 60.5 (C^1); 57.2, 50.3 (NMe_2). Crystals suitable for X-ray analysis were collected by slow diffusion of pentane into a diethyl ether solution of **3 a** at -30°C .

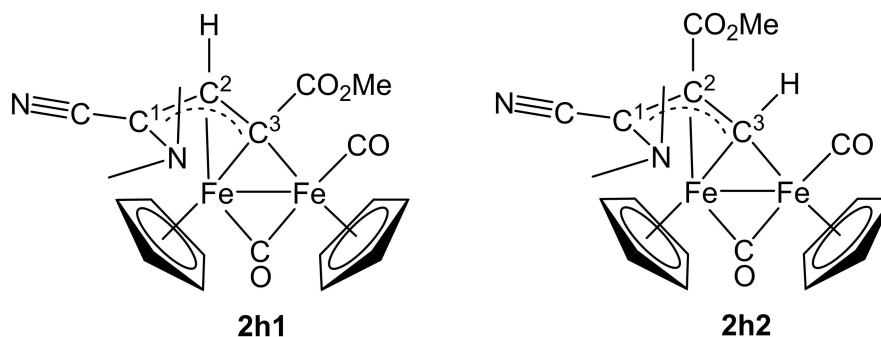


Figure 4. Structures of **2h1** and **2h2**.

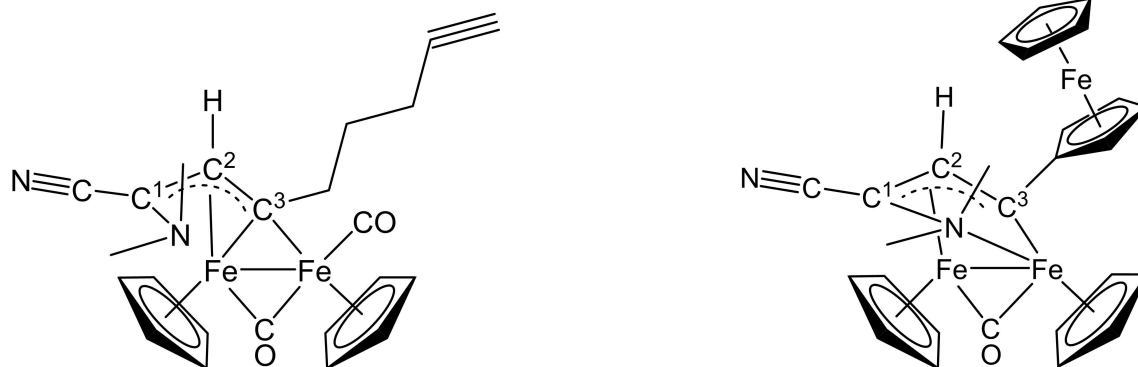


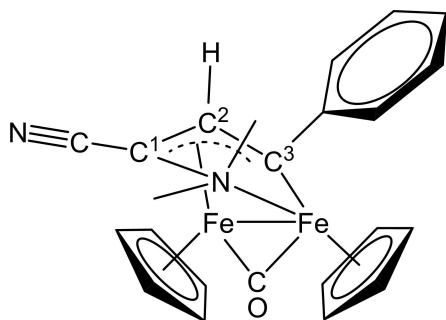
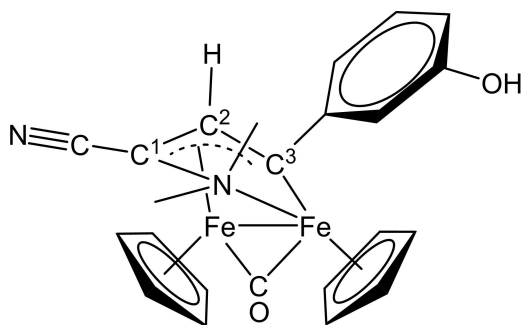
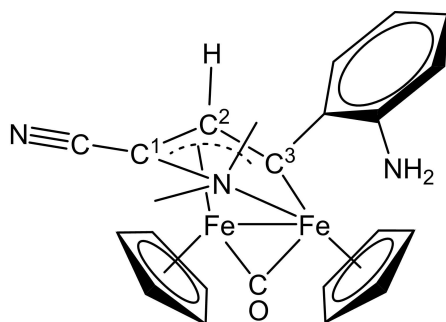
Figure 5. Structure of **2i**.

Figure 6. Structure of **3 a**.

[Fe₂Cp₂(μ-CO){μ-k³C,kN-C³(Ph)C²HC¹(CN)NMe₂}], 3 b (Figure 7)

From **2b** (240 mg, 0.498 mmol). Reaction time: 48 h. Chromatography: Et₂O. Brown solid. Yield 147 mg (65%). Anal. calcd. for C₂₃H₂₂Fe₂N₂O: C, 60.83; H, 4.88; N, 6.17. Found: C, 60.97; H, 4.72; N, 6.28. IR (CH₂Cl₂): $\tilde{\nu}/\text{cm}^{-1}$ = 2197w-m (C≡N), 1750s (μ-CO), 1591w (arom CC). ¹H NMR (CDCl₃): δ/ppm = 7.51, 7.45, 7.35 (m, 5 H, Ph), 5.91 (s, 1 H, C²H); 4.26, 4.02 (s, 10 H, Cp); 2.15, 1.40 (s, 6 H, NMe₂). ¹³C {¹H} NMR (CDCl₃): δ/ppm = 283.5 (μ-CO); 187.4 (C³); 158.4 (*ipso*-Ph); 128.4, 128.0, 125.8 (Ph); 119.5 (C≡N); 84.3, 83.9 (Cp); 80.4 (C²); 61.7 (C¹); 57.4, 50.5 (NMe₂).

A mixture of NaBH₄ (14 mg, 0.37 mmol) and **3b** (20 mg, 0.044 mmol) in THF (5 mL), under N₂ atmosphere, was stirred for 4 hours at room temperature and 1 additional hour at 50 °C. IR analysis of the final solution pointed out the presence of **3b** as the only organo-iron compound.

Figure 7. Structure of **3b**.Figure 8. Structure of **3c**.Figure 9. Structure of **3d**.**[Fe₂Cp₂(μ-CO){μ-k³C,kN-C³(3-C₆H₄OH)C²HC¹(CN)NMe₂}], 3 c (Figure 8)**

From **2c** (178 mg, 0.357 mmol). Reaction time: 12 h. Chromatography: THF. Brown solid. Yield 148 mg (88%). Anal. calcd. for C₂₃H₂₂Fe₂N₂O₂: C, 57.76; H, 4.72; N, 5.96. Found: C, 57.55; H, 4.65; N, 5.82. IR (CH₂Cl₂): $\tilde{\nu}/\text{cm}^{-1}$ = 2197w (C≡N), 1751vs (μ-CO), 1603 m, 1585 m, 1576w. ¹H NMR (CDCl₃): δ/ppm = 7.31, 7.10, 7.04, 6.86 (m, 4 H, C₆H₄); 5.92 (s, 1 H, C²H); 4.29, 4.07 (s, 10 H, Cp); 2.17, 1.39 (s, 6 H, NMe₂). ¹³C {¹H} NMR (CDCl₃): δ/ppm = 283.2 (μ-CO); 186.3 (C³); 160.1, 155.5, 129.0, 121.1, 115.1, 112.7 (C₆H₄); 119.5 (C≡N); 84.3, 83.9 (Cp); 80.2 (C²); 61.7 (C¹); 57.3, 50.4 (NMe₂).

[Fe₂Cp₂(μ-CO){μ-k³C,kN-C³(2-C₆H₄NH₂)C²HC¹(CN)NMe₂}], 3 d (Figure 9)

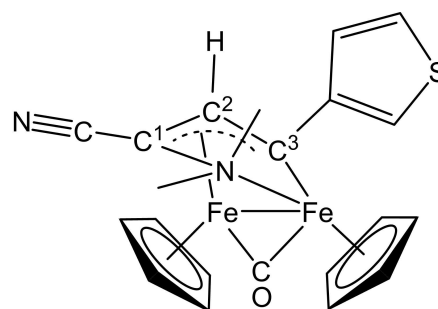
From **2d** (140 mg, 0.267 mmol). Reaction time: 16 h. Chromatography: Et₂O. Brown solid. Yield 74 mg (59%). Anal. calcd. for C₂₃H₂₃Fe₂N₃O: C, 58.88; H, 4.94; N, 8.96. Found: C, 58.60; H, 4.75; N, 9.05. IR (CH₂Cl₂): $\tilde{\nu}/\text{cm}^{-1}$ = 2198w-m (C≡N), 1751vs (μ-CO). ¹H NMR (CDCl₃): δ/ppm = 8.23, 7.30, 7.03, 6.70, (m, 4 H, C₆H₄); 5.96 (s, 1 H, C²H); 4.33, 4.08 (s, 10 H, Cp); 3.11 (s, 2H, NH₂); 2.19, 1.51 (s, 6 H, NMe₂). ¹³C {¹H} NMR (CDCl₃): δ/ppm = 280.9 (μ-CO); 179.2 (C³); 143.4, 141.4, 128.3, 127.0, 117.8, 115.8 (C₆H₄); 119.7 (C≡N); 85.1, 84.2 (Cp); 81.2 (C²); 61.5 (C¹); 57.0, 50.9 (NMe₂).

[Fe₂Cp₂(μ-CO){μ-k³C,kN-C³(C₄H₃S)C²HC¹(CN)NMe₂}], 3 e (Figure 10)

From **2e** (234 mg, 0.480 mmol). Reaction time: 48 h. Chromatography: CH₂Cl₂. Brown solid. Yield 214 mg (97%). Anal. calcd. for C₂₁H₂₀Fe₂N₂OS: C, 54.81; H, 4.38; N, 6.09. Found: C, 54.70; H, 4.27; N, 6.13. IR (CH₂Cl₂): $\tilde{\nu}/\text{cm}^{-1}$ = 2197 m (C≡N), 1750s (μ-CO). ¹H NMR (CDCl₃): δ/ppm = 7.58, 7.37, 6.80 (s, 3 H, C₄H₃S); 5.93 (s, 1 H, C²H); 4.22, 4.07 (s, 10 H, Cp); 2.13, 1.37 (s, 6 H, NMe₂). ¹³C {¹H} NMR (CDCl₃): δ/ppm = 283.7 (μ-CO); 179.2 (C³); 159.8 (*ipso*-C₄H₃S); 130.9, 125.2, 115.7 (C₃H₃S); 119.4 (C≡N); 84.0, 83.7 (Cp); 80.8 (C²); 61.6 (C¹); 57.4, 50.8 (NMe₂).

[Fe₂Cp₂(μ-CO){μ-k³C,kN-C³(Me)C²HC¹(CN)NMe₂}], 3 f (Figure 11)

From **2f** (31 mg, 0.074 mmol). Reaction time: 24 h. Chromatography: Et₂O. Dark- brown solid. Yield 23 mg (79%). Anal. calcd. for C₁₈H₂₀Fe₂N₂O: C, 55.14; H, 5.14; N, 7.15. Found: C, 54.92; H, 5.23; N, 7.03. IR (CH₂Cl₂): $\tilde{\nu}/\text{cm}^{-1}$ = 2193w-m (C≡N), 1746vs (μ-CO). ¹H NMR (CDCl₃): δ/ppm = 5.80 (s, 1 H, C²H); 4.21, 4.16 (s, 10 H, Cp); 3.91 (s, 3 H, C³Me); 2.08, 1.28 (s, 6 H, NMe₂). ¹³C {¹H} NMR (CDCl₃): δ/ppm = 285.9 (μ-CO); 192.5 (C³); 119.7 (C≡N); 84.1 (C²); 83.2, 82.7 (Cp); 59.9 (C¹); 57.1, 50.2 (NMe₂); 38.0 (C³Me).

Figure 10. Structure of **3e**.

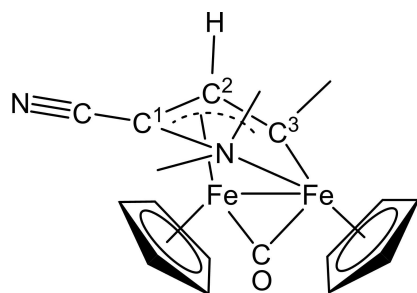


Figure 11. Structure of 3f.

[Fe₂Cp₂(μ-CO){μ-k³C,kN-C³(SiMe₃)C²HC¹(CN)NMe₂}], 3g (Figure 12)

From **2g** (156 mg, 0.326 mmol). Reaction time: 12 h. Chromatography: Et₂O. Dark-brown solid. Yield 135 mg (92%). Anal. calcd. for C₂₀H₂₆Fe₂N₂O₂Si: C, 53.36; H, 5.82; N, 6.22. Found: C, 53.05; H, 5.98; N, 6.04. IR (CH₂Cl₂): $\tilde{\nu}/\text{cm}^{-1}$ = 2195 m (C≡N), 1748 s (μ-CO). ¹H NMR (CDCl₃): δ/ppm = 6.06 (s, 1 H, C²H); 4.28, 4.26 (s, 10 H, Cp); 2.08, 1.22 (s, 6 H, NMe₂); 0.60 (s, 9 H, SiMe₃). ¹³C{¹H} NMR (CDCl₃): δ/ppm = 282.8 (μ-CO); 180.7 (C³); 119.8 (C≡N); 82.5, 82.2 (Cp); 81.0 (C²); 62.6 (C¹); 57.0, 50.3 (NMe₂); 2.7 (SiMe₃).

[Fe₂Cp₂(μ-CO){μ-k³C,kN-C³(CO₂Me)C²HC¹(CN)NMe₂}], 3h (Figure 13)

From **2h1** (99 mg, 0.21 mmol). Reaction time: 12 h. Chromatography: Et₂O. Dark-brown solid. Yield 87 mg (94%). Anal. calcd. for C₁₉H₂₀Fe₂N₂O₃: C, 52.33; H, 4.62; N, 6.42. Found: C, 52.11; H, 4.76; N, 6.26. IR (CH₂Cl₂): $\tilde{\nu}/\text{cm}^{-1}$ = 2201 w-m (C≡N), 1763 s (μ-CO), 1694 (CO₂Me), 1670 m (CO₂Me). ¹H NMR (CDCl₃): δ/ppm = 6.23 (s, 1 H, C²H); 4.33, 4.30 (s, 10 H, Cp); 4.08 (s, 3 H, CO₂Me); 2.13, 1.29 (s, 6 H, NMe₂). ¹³C{¹H} NMR (CDCl₃): δ/ppm = 279.2 (μ-CO); 181.3 (C³); 162.6

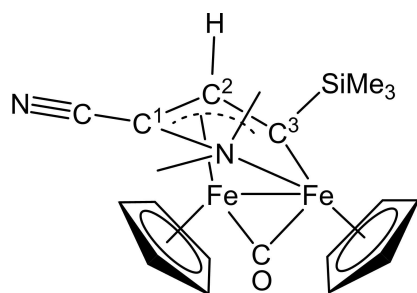


Figure 12. Structure of 3g.

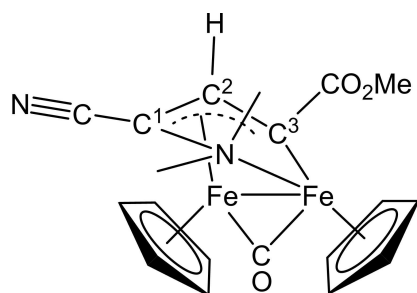


Figure 13. Structure of 3h.

(CO₂Me); 118.7 (C≡N); 83.6, 82.7 (Cp); 83.2 (C_p); 62.2 (C¹); 57.5, 50.4 (NMe₂); 52.1 (CO₂Me).

Thermal treatment of **2h2** (isopropanol, reflux temperature, 5 days) did not result in any reaction.

[Fe₂Cp₂(μ-CO){μ-k³C,kN-C³(CH₂CH₂CH₂CCH)C²HC¹(CN)NMe₂}], 3i (Figure 14)

From **2i** (83 mg, 0.176 mmol). Reaction time: 72 h. Chromatography: Et₂O. Dark-brown solid. Yield 69 mg (88%). Anal. calcd. for C₂₂H₂₄Fe₂N₂O: C, 59.50; H, 5.45; N, 6.31. Found: C, 59.21; H, 5.61; N, 6.19. IR (CH₂Cl₂): $\tilde{\nu}/\text{cm}^{-1}$ = 2193 w (C≡N), 1746 s, 1735 m (μ-CO). ¹H NMR (CDCl₃): δ/ppm = 5.84 (s, 1 H, C²H); 4.24, 4.21 (s, 10 H, Cp); 4.13, 4.03, 3.06, 2.78 (m, 6 H, 3×CH₂); 2.14 (t, ⁴J_{HH} = 2.4 Hz, 1H, ≡CH); 2.09, 1.28 (s, 6 H, NMe₂). ¹³C{¹H} NMR (CDCl₃): δ/ppm = 285.3 (μ-CO); 194.6 (C³); 119.7 (C≡N); 83.3, 82.5 (Cp); 84.7 (C≡CH); 69.3 (C≡CH); 83.1 (C²); 60.4 (C¹); 57.0, 50.1 (NMe₂); 50.6, 32.6, 19.3 (3×CH₂).

[Fe₂Cp₂(μ-CO){μ-k³C,kN-C³(Me)C²(Me)C¹(CN)NMe₂}], 3j (Figure 15)

From **2j** (171 mg, 0.394 mmol). Reaction time: 16 h. Chromatography: CH₂Cl₂/THF (9:1 v/v). Brown solid. Yield 77 mg (48%). Anal. calcd. for C₁₉H₂₂Fe₂N₂O: C, 56.20; H, 5.46; N, 6.90. Found: C, 56.02; H, 5.28; N, 6.80. IR (CH₂Cl₂): $\tilde{\nu}/\text{cm}^{-1}$ = 2192 w-m (C≡N), 1743 s (μ-CO). ¹H NMR (CDCl₃): δ/ppm = 4.14, 4.11 (s, 10 H, Cp); 3.81 (s, 3 H, C³Me); 2.42 (s, 3 H, C²Me); 2.00, 1.22 (s, 6 H, NMe₂). ¹³C{¹H} NMR (CDCl₃): δ/ppm = 287.2 (μ-CO); 187.6 (C³); 119.8 (C≡N); 95.2 (C²); 84.0, 82.9 (Cp); 61.5 (C¹); 56.6, 49.7 (NMe₂); 34.5 (C³Me); 25.7 (C²Me). Crystals suitable for X-ray analysis were obtained by slow diffusion of diethyl ether into a CH₂Cl₂ solution of **3j** at -30°C.

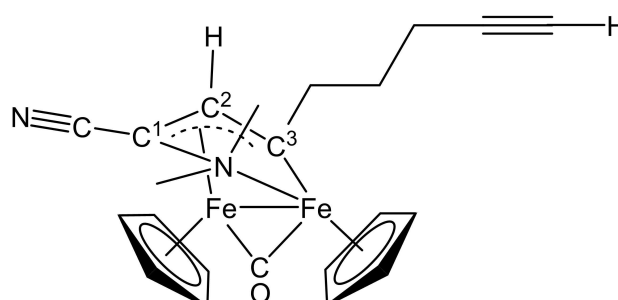


Figure 14. Structure of 3i.

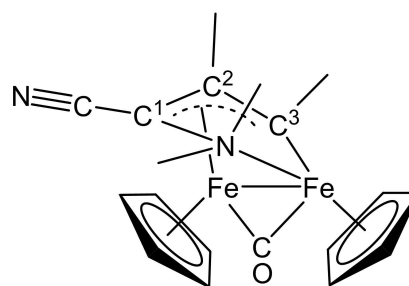


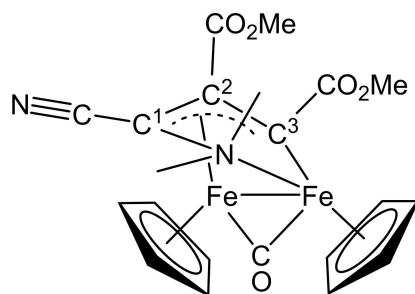
Figure 15. Structure of 3j.

[Fe₂Cp₂(μ-CO){μ-k³C,kN-C³(CO₂Me)C²(CO₂Me)C¹(CN)NMe₂}], 3k (Figure 16)

From **2k** (152 mg, 0.291 mmol). Reaction time: 48 h. Chromatography: THF. Dark-brown solid. Yield 81 mg (56%). Anal. calcd. for C₃₁H₂₂Fe₂N₂O₅: C, 51.05; H, 4.49; N, 5.67. Found: C, 50.86; H, 4.60; N, 5.58. IR (CH₂Cl₂): $\tilde{\nu}/\text{cm}^{-1}$ = 2202w (C≡N), 1774 m (μ-CO), 1743 s, 1711 s (CO₂Me). ¹H NMR (CDCl₃): δ/ppm = 6.94 (s, 1 H, C²H); 4.43, 4.23 (s, 10 H, Cp); 4.16, 3.91 (s, 6 H, CO₂Me); 2.11, 1.37 (s, 6 H, NMe₂). ¹³C{¹H} NMR (CDCl₃): δ/ppm = 274.5 (μ-CO); 182.0, 169.6 (CO₂Me); 177.8 (C³); 125.6 (C≡N); 85.7, 83.9 (Cp); 79.5 (C²); 59.3 (C¹); 56.8, 50.0 (NMe₂); 52.6, 52.3 (CO₂Me). Crystals suitable for X-ray analysis were obtained by slow diffusion of diethyl ether into a CH₂Cl₂ solution of **3k** at -30 °C.

[Fe₂Cp₂(μ-CO){μ-k³C,kN-C³(Fc)C²HC¹(CN)N(Me)(Cy)}], 3l (Figure 17)

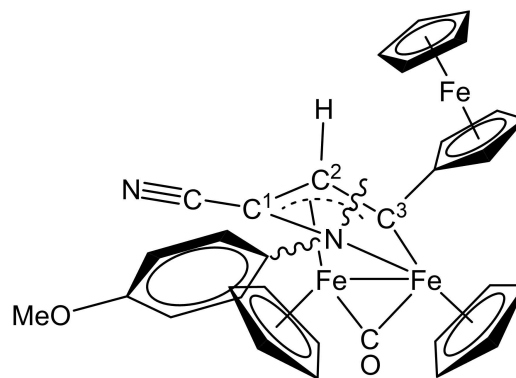
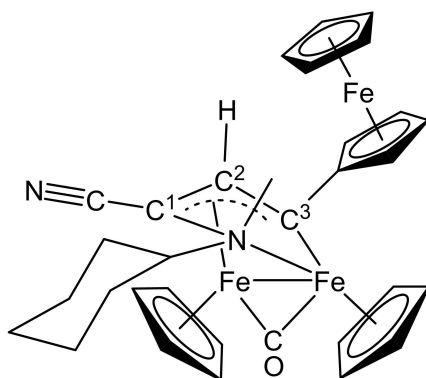
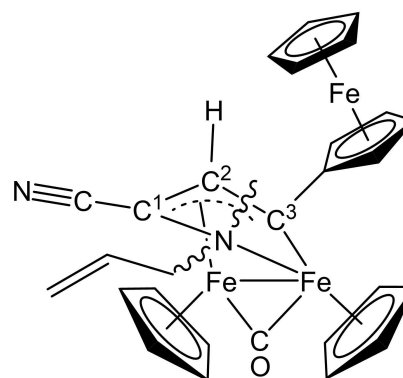
From **2l** (151 mg, 0.229 mmol). Reaction time: 4 h. Chromatography: CH₂Cl₂. Brown-red solid. Yield 122 mg (85%). Anal. calcd. for C₃₂H₃₄Fe₂N₂O: C, 61.00; H, 5.44; N, 4.45. Found: C, 60.76; H, 5.51; N, 4.55. IR (CH₂Cl₂): $\tilde{\nu}/\text{cm}^{-1}$ = 2193w-m (C≡N), 1742vs (μ-CO). ¹H NMR (CDCl₃): δ/ppm = 6.20 (s, 1 H, C²H); 4.67, 4.12 (m, 4 H, C₅H₄); 4.49, 4.00 (s, 10 H, Cp); 4.40 (s, 5 H, Cp^{Fc}); 2.26 (s, 3 H, NMe); 2.08, 1.81, 1.64, 1.51, 1.22 (m, 11 H, C₆H₁₁). ¹³C{¹H} NMR (CDCl₃): δ/ppm = 286.3 (μ-CO); 182.6 (C³); 122.0 (C≡N); 108.0 (*ipso*-C₅H₄); 83.1 (C²); 84.6, 83.5 (Cp); 69.0 (Cp^{Fc}); 75.0 (*ipso*-C₅H₄); 69.6, 68.0, 67.9, 67.5 (C₅H₄); 55.5 (C¹); 44.9 (NMe); 30.4, 29.0, 26.4, 26.1, 25.7 (CH^{Cy} + CH₂^{Cy}). Crystals suitable for X-ray analysis were obtained by slow diffusion of pentane into a CH₂Cl₂ solution of **3l** at -30 °C.

Figure 16. Structure of **3k**.**[Fe₂Cp₂(μ-CO){μ-k³C,kN-C³(Fc)C²HC¹(CN)N(Me)(4-C₆H₄OMe)}], 3m (Figure 18)**

From **2m** (115 mg, 0.169 mmol). Reaction time: 16 h. Chromatography: Et₂O. Brown solid. Yield 49 mg (44%). Anal. calcd. for C₃₃H₃₀Fe₂N₂O₂: C, 60.59; H, 4.62; N, 4.28. Found: C, 60.42; H, 4.70; N, 4.39. IR (CH₂Cl₂): $\tilde{\nu}/\text{cm}^{-1}$ = 2196w (C≡N), 1749 s (μ-CO), 1611w (arom C), 1586w (C²). ¹H NMR (CDCl₃): δ/ppm = 6.61, 6.46 (s, 1 H, C²H); 4.54, 4.46, 3.85, 3.82 (s, 10 H, Cp); 4.51, 4.46 (s, 5 H, Cp^{Fc}); 3.73, 3.73 (s, 3 H, OMe); 2.89, 1.97 (s, 3 H, NMe). Isomer ratio = 1.7. ¹³C{¹H} NMR (CDCl₃): δ/ppm = 285.0, 280.4 (μ-CO); 183.9, 181.9 (C³); 156.5, 146.1, 156.5, 143.0 (*ipso*-C₆H₄); 125.6, 125.4 (C≡N); 121.5, 120.9, 120.1, 120.0, 115.0, 113.7, 113.0 (C₆H₄); 107.6, 107.1 (*ipso*-C₅H₄); 86.3 (C²); 84.3, 84.3, 84.2, 83.5 (Cp); 70.1, 69.9, 69.1, 69.0, 68.9, 68.7, 68.2, 68.1 (C₅H₄); 69.1, 69.0 (Cp^{Fc}); 67.5, 67.3 (C¹); 55.9, 55.5 (OMe); 56.5, 51.8 (NMe).

[Fe₂Cp₂(μ-CO){μ-k³C,kN-C³(Fc)C²HC¹(CN)N(Me)(CH₂CHCH₂)}], 3n (Figure 19)

From **2n** (177 mg, 0.287 mmol). Reaction time: 16 h. Chromatography: Et₂O. Red-brown solid. Yield 149 mg (88%). Anal. calcd. for C₂₉H₂₈Fe₂N₂O: C, 59.23; H, 4.80; N, 4.76. Found: C, 59.42; H, 4.70; N, 4.59. IR (CH₂Cl₂): $\tilde{\nu}/\text{cm}^{-1}$ = 2195 m (C≡N), 1747vs (μ-CO). ¹H NMR (CDCl₃): δ/ppm = 6.22, 6.22 (s, 1 H, C²H); 5.87, 5.60 (m, 1 H, CH=); 5.23, 5.21, 5.20, 5.18, 5.17, 5.14, 5.01, 4.98 (m, 2 H, =CH₂); 4.91, 4.82, 4.54, 4.48, 3.96, 3.83 (s, 4 H, C₅H₄); 4.51, 4.46, 3.96, 3.90 (s, 10 H, Cp); 4.48, 4.48 (s, 5 H, Cp^{Fc}); 3.60, 2.50, 2.15, 1.85 (m, 2 H, NCH₂); 2.17, 1.24 (s, 3 H, NMe). ¹³C{¹H} NMR (CDCl₃): δ/ppm = 284.4, 283.5 (μ-CO); 185.2, 184.8 (C³); 132.0, 129.7 (CH=); 121.9, 121.6 (=CH₂); 121.1, 120.4 (C≡N); 108.6, 108.0 (*ipso*-C₅H₄); 83.8, 83.8, 83.7, 83.2 (Cp); 83.0, 82.4 (C²); 72.2, 63.6 (NCH₂); 70.2, 69.7, 69.2, 68.4, 68.0, 67.9, 67.5,

Figure 18. Structure of **3m** (wavy bonds indicate stereoisomers).Figure 17. Structure of **3l**.Figure 19. Structure of **3n** (wavy bonds indicate stereoisomers).

67.3 (C₅H₄); 68.9, 68.9 (Cp^{Fc}); 60.9, 57.2 (C¹); 53.2, 46.6 (NMe). Isomer ratio = 1.

[Fe₂Cp₂(μ-CO){μ-k³C,kN-C³(Fc)C²HC¹(CN)N(Me)(CH₂Ph)}], **3 o** (Figure 20)

From **2 o** (68 mg, 0.102 mmol). Reaction time: 18 h. Chromatography: Et₂O/CH₂Cl₂ (9:1 v/v). Brown solid. Yield 48 mg (73%). Anal. calcd. for C₃₃H₃₀Fe₃N₂O: C, 62.11; H, 4.74; N, 4.39. Found: C, 61.52; H, 4.84; N, 4.44. IR (THF): $\tilde{\nu}/\text{cm}^{-1}$ = 2194 m (C≡N), 1747 s (μ-CO). IR (DCM): $\tilde{\nu}/\text{cm}^{-1}$ = 2193 m (C≡N), 1743 s (μ-CO). ¹H NMR (CDCl₃): δ/ppm = 7.66, 7.50–7.20, 7.07 (m, 5 H, C₆H₅); 6.43, 6.31 (s, 1 H, C²H); 4.94, 4.86, 4.61, 4.49, 4.09, 3.87 (m, 4 H, C₅H₄); 4.58, 4.58, 4.07, 3.53 (s, 10 H, Cp); 4.52, 4.47 (s, 5 H, Cp^{Fc}); 4.00, 3.20, 2.70, 2.34 (d, ²J = 12.9, 12.1 Hz, 2 H, NCH₂); 2.20, 1.49 (s, 6 H, NMe). ¹³C{¹H} NMR (CDCl₃): δ/ppm = 284.3 (μ-CO); 185.1, 184.6 (C³); 134.7, 132.5, 131.5, 130.1, 129.0, 128.6, 128.4, 128.0 (C₆H₅); 120.5, 119.6 (C≡N); 108.9, 108.0 (*ipso*-C₅H₄); 83.9, 83.8, 83.7, 83.4 (Cp); 82.9, 82.4 (C²); 72.8, 63.6 (NCH₂); 70.0, 69.9, 68.2, 68.0, 67.8, 67.6, 67.5 (C₅H₄); 68.9, 68.8 (Cp^{Fc}); 61.4, 56.5 (C¹); 54.2, 45.5 (NMe). Isomer ratio = 1.

1.3) Synthesis and isolation of [FeCp(CO){C¹NMe₂C²HC³(2-C₆H₄NH₂)C(=O)}], **4** (Figure 21)

This compound was obtained as a by-product, separated by alumina chromatography, of the reaction leading to **4 d**. Chromatography: THF. Brown solid. Yield 21 mg (26%). Anal. calcd. for C₁₈H₁₈FeN₂O₂: C, 61.74; H, 5.18; N, 8.00. Found: C, 61.54; H, 5.12; N, 7.83. IR (CH₂Cl₂): ν/cm^{-1} = 1917 s (CO), 1618 m (CO_{acyl}), 1599 (C=C). ¹H NMR (CDCl₃): δ/ppm = 7.59 (s, 1 H, C²H); (7.11, 6.70 (m, 4 H, C₆H₄); 4.56 (s, 5 H, Cp); 4.13 (s, 2 H, NH₂); 3.73, 3.50 (s, 6 H, NMe₂). ¹³C{¹H} NMR (CDCl₃): δ/ppm = 273.6 (CO_{acyl}); 261.5 (C¹); 222.0 (CO); 173.3 (C³); 149.2 (C²); 145.6, 130.3, 122.0, 118.3, 117.4 (C₆H₄); 85.2 (Cp);

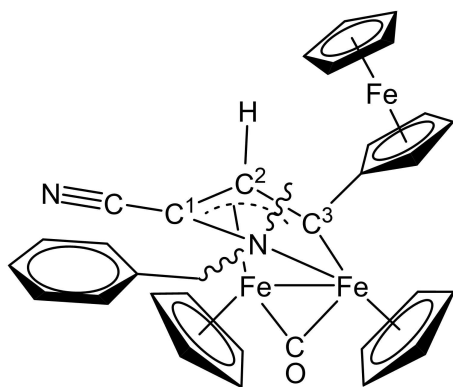


Figure 20. Structure of **3 o** (wavy bonds indicate stereoisomers).

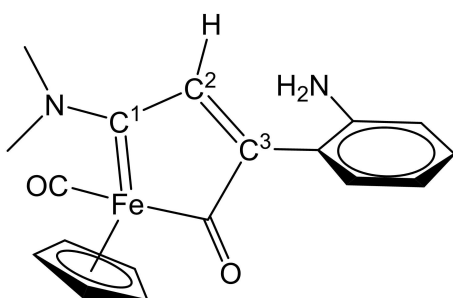


Figure 21. Structure of **4**.

51.7, 43.3 (NMe₂). Crystals suitable for X-ray analysis were obtained by slow diffusion of hexane into a CH₂Cl₂ solution of **4** at –30 °C.

2) X-ray Crystallography

Crystal data and collection details for **3 a**, **3 j**, **3 k**, **3 l**·CH₂Cl₂ and **4**·CH₂Cl₂ are reported in Table 5. Data were recorded on a Bruker APEX II diffractometer equipped with a PHOTON100 detector using Mo–K α radiation. Data were corrected for Lorentz polarization and absorption effects (empirical absorption correction SADABS).^[72] The structures were solved by direct methods and refined by full-matrix least-squares based on all data using F².^[73] The crystals of **3 a** are racemically twinned and restraints have been used during the refinement. Even though the overall connectivity and stereochemistry is well-established, bond precision is not very high, especially when light C atoms are involved. Thus, all the discussion concerning bonding parameters are based on the related complexes **3 j**, **3 k**, and **3 l**·CH₂Cl₂.

3) Hydroboration Reactions

General procedure. A 10 mL oven-dried Schlenk tube equipped with a stirring bar was charged with 0.25 mmol of the selected carbonyl compound and 10 μL of dodecane (internal standard for GC). A freshly prepared 10 mM stock solution of catalyst **3** (2.5–5.0 μmol , 1–2 mol%) in the reaction solvent (250–500 μL) was added under N₂ atmosphere. Dry, degassed solvent was then added to reach a total reaction volume of 0.5 mL. Pinacolborane (53 μL , 0.375 mmol, 1.5 equiv.) was subsequently added. The tube was sealed, purged three times with N₂, and then pressurized with 1 atm of N₂. The reaction mixture was stirred at room temperature for the time indicated in Tables 2–4. Reaction progress was monitored by GC-FID analysis. Aliquots of 20 μL were withdrawn from the reaction mixture, diluted with 980 μL of ethyl acetate, and analysed by GC-FID. After completion of the reaction, 350 μL of the reaction mixture was transferred into an NMR tube containing 50 μL of C₆D₆ and 1,3,5-trimethoxybenzene (external standard). ¹H NMR analysis was performed to determine the selectivity. The signals corresponding to the residual starting material and the product (–CRHBPin) were integrated and compared to the signal of the aromatic C–H protons of the internal standard for yield calculation.

Supporting Information Available

X-ray structure of **4** (Figure S1); NMR spectra of iron complexes (Figures S2–S40) and borate esters (Charts S1–S19); representative NMR spectrum for selectivity determination (Figure S41); comparative view of spectroscopic data (Table S1); electrochemical study of **3 n** (Figure S42); details of epoxide/CO₂ coupling reactions. CCDC reference numbers 2350495 (**3 a**), 2350496 (**3 j**), 2350497 (**3 k**), 2350498 (**3 l**) and 2350499 (**4**) contain the supplementary crystallographic data for the X-ray studies reported in this paper. These data can be obtained free of charge at www.ccdc.cam.ac.uk/conts/retrieving.html (or from the Cambridge Crystallographic Data Centre, 12, Union Road, Cambridge CB2 1EZ, UK; fax: (internat.) +44-1223/336-033; e-mail: deposit@ccdc.cam.ac.uk).

Table 5. Crystal data and measurement details for **3 a**, **3 j**, **3 k**, **3 l**·CH₂Cl₂ and **4**·CH₂Cl₂.

	3 a	3 j	3 k	3 l ·CH ₂ Cl ₂	4 ·CH ₂ Cl ₂
Formula	C ₂₇ H ₂₆ Fe ₃ N ₂ O	C ₁₉ H ₂₂ Fe ₂ N ₂ O	C ₂₁ H ₂₂ Fe ₂ N ₂ O ₅	C ₃₃ H ₃₆ Cl ₂ Fe ₃ N ₂ O	C ₁₉ H ₂₀ Cl ₂ FeN ₂ O ₂
FW	562.05	406.08	494.10	715.09	435.12
T, K	100(2)	100(2)	100(2)	100(2)	100(2)
λ, Å	0.71073	0.71073	0.71073	0.71073	0.71073
Crystal system	Orthorhombic	Monoclinic	Monoclinic	Triclinic	Orthorhombic
Space group	<i>Pna</i> 2 ₁	<i>P</i> ₂ ₁ / <i>c</i>	<i>P</i> ₂ ₁ / <i>c</i>	<i>P</i> $\bar{1}$	<i>Pbca</i>
<i>a</i> , Å	12.5043(14)	9.5946(5)	8.4574(5)	10.3306(5)	21.390(5)
<i>b</i> , Å	12.9828(13)	14.9919(7)	15.5841(9)	11.3960(5)	7.5959(5)
<i>c</i> , Å	14.0587(14)	11.7095(6)	15.1825(9)	13.9861(6)	22.8471(15)
α, °	90	90	90	73.6520(10)	90
β, °	90	93.925(2)	99.449(2)	71.7950(10)	90
γ, °	90	90	90	72.062(2)	90
Cell Volume, Å ³	2282.3(4)	1680.36(15)	1973.9(2)	1456.50(12)	3712.1(4)
Z	4	4	4	2	8
<i>D</i> _c , g·cm ⁻³	1.636	1.605	1.663	1.631	1.557
μ, mm ⁻¹	1.905	1.734	1.507	1.689	1.117
F(000)	1152	840	1016	736	1792
Crystal size, mm	0.20×0.16×0.13	0.24×0.21×0.18	0.22×0.19×0.15	0.16×0.13×0.11	0.16×0.12×0.08
θ limits, °	2.135–26.994	2.128–27.000	1.886–26.000	1.566–25.997	1.783–25.095
Reflections collected	45532	25652	20108	20445	43946
Independent reflections	4967 [<i>R</i> _{int} = 0.0520]	3664 [<i>R</i> _{int} = 0.0313]	3878 [<i>R</i> _{int} = 0.0389]	5689 [<i>R</i> _{int} = 0.0312]	3301 [<i>R</i> _{int} = 0.0600]
Data/restraints /parameters	4967/163/283	3664/0/221	3878/0/275	5689/0/371	3301/44/243
Goodness on fit on F ²	1.031	1.093	1.029	1.073	1.153
<i>R</i> ₁ (<i>I</i> > 2σ(<i>I</i>))	0.0427	0.0212	0.0271	0.0338	0.0881
<i>wR</i> ₂ (all data)	0.1101	0.0527	0.0675	0.0748	0.2271
Largest diff. peak and hole, e Å ⁻³	1.254/−1.105	0.385/−0.327	0.402/−0.306	0.922/−0.768	1.857/−1.447

Acknowledgements

We gratefully thank the University of Pisa for financial support (Fondi di Ateneo 2021). ADG acknowledges the University of L'Aquila for financial support under the program "Progetti di ricerca di Ateneo 2021–2022". ADG and MC greatly thank the European Union - NextGenerationEU under the Italian Ministry of University and Research (MUR) National Innovation Ecosystem grant ECS00000041 – VITALITY – CUP E13C22001060006, for financial support. Open Access publishing facilitated by Università degli Studi dell'Aquila, as part of the Wiley - CRUI-CARE agreement.

Conflict of Interests

The authors declare no conflict of interest.

Data Availability Statement

The data that support the findings of this study are available from the corresponding author upon reasonable request.

Keywords: diiron complexes · homogeneous catalysis · cooperative effects · allylidene ligand · hydroboration reaction

- [1] W. Matsuoka, Y. Harabuchi, S. Maeda, *ACS Catal.* **2023**, *13*, 5697–5711.
- [2] W. Wang, G. B. Hammond, B. Xu, *J. Am. Chem. Soc.* **2012**, *134*, 5697–5705.
- [3] A. Fürstner, *ACS Cent. Sci.* **2016**, *2*, 778–789.
- [4] I. Bauer, H.-J. Knölker, *Chem. Rev.* **2015**, *115*, 3170–3387.
- [5] D. Wei, C. Darcel, *Chem. Rev.* **2019**, *119*, 2550–2610.
- [6] D. R. Pye, N. P. Mankad, *Chem. Sci.* **2017**, *8*, 1705–1718.
- [7] J. Campos, *Nat. Chem. Rev.* **2020**, *4*, 696–702.
- [8] V. Ritleng, M. J. Chetcuti, *Chem. Rev.* **2007**, *107*, 797–858.
- [9] R. Govindarajan, S. Deolka, J. R. Khusnutdinova, *Chem. Sci.* **2022**, *13*, 14008–14031.
- [10] C. M. Farley, C. Uyeda, *Trends Chem.* **2019**, *1*(5), 497–509.
- [11] G. Berggren, A. Adamska, C. Lambert, T. R. Simmons, J. Esselborn, M. Atta, S. Gambarelli, J.-M. Mouesca, E. Reijerse, W. Lubitz, T. Happe, V. Artero, M. Fontecave, *Nature* **2013**, *499*, 66–69.
- [12] R. Mazzoni, M. Salmi, V. Zanotti, *Chem. Eur. J.* **2012**, *18*, 10174–10194.
- [13] L. Biancalana, F. Marchetti, *Coord. Chem. Rev.* **2021**, *449*, 214203.
- [14] C. P. Casey, E. A. Austin, *J. Am. Chem. Soc.* **1988**, *110*, 7106–7113.
- [15] F. Arrigoni, L. Bertini, L. De Gioia, A. Cingolani, R. Mazzoni, V. Zanotti, G. Zampella, *Inorg. Chem.* **2017**, *56*, 13852–13864.
- [16] G. Bresciani, L. Biancalana, S. Zacchini, G. Pampaloni, G. Ciancaleoni, F. Marchetti, *Appl. Organomet. Chem.* **2023**, *37*, e6990.
- [17] S. Schoch, S. Braccini, L. Biancalana, A. Pratesi, T. Funaioli, S. Zacchini, G. Pampaloni, F. Chiellini, F. Marchetti, *Inorg. Chem. Front.* **2022**, *9*, 5118–5139.

- [18] D. Rocco, L. K. Batchelor, G. Agonigi, S. Braccini, F. Chiellini, S. Schoch, T. Biver, T. Funaioli, S. Zacchini, L. Biancalana, M. Ruggeri, G. Pampaloni, P. J. Dyson, F. Marchetti, *Chem. Eur. J.* **2019**, *25*, 14801–14816.
- [19] B. Campanella, S. Braccini, G. Bresciani, M. De Franco, V. Gandin, F. Chiellini, A. Pratesi, G. Pampaloni, L. Biancalana, F. Marchetti, *Metalomics* **2023**, *15*, mfac096.
- [20] D. Rocco, N. Busto, C. Pérez-Araiz, L. Biancalana, S. Zacchini, G. Pampaloni, B. Garcia, F. Marchetti, *Appl. Organomet. Chem.* **2020**, *34*, e5923.
- [21] G. Bresciani, G. Ciancaleoni, S. Zacchini, L. Biancalana, G. Pampaloni, T. Funaioli, F. Marchetti, *Dalton Trans.* **2024**, *53*, 4299–4313.
- [22] S. Braccini, G. Rizzi, L. Biancalana, A. Pratesi, S. Zacchini, G. Pampaloni, F. Chiellini, F. Marchetti, *Pharmaceutica* **2021**, *13*, 1158.
- [23] S. Schoch, G. Bresciani, C. Saviozzi, T. Funaioli, M. Bortoluzzi, G. Pampaloni, F. Marchetti, *New J. Chem.* **2023**, *47*, 8828–8844.
- [24] V. G. Albano, L. Busetto, F. Marchetti, M. Monari, S. Zacchini, V. Zanotti, *C. Organomet. Chem.* **2006**, *691*, 4234–4243.
- [25] S. Schoch, L. K. Batchelor, T. Funaioli, G. Ciancaleoni, S. Zacchini, S. Braccini, F. Chiellini, T. Biver, G. Pampaloni, P. J. Dyson, F. Marchetti, *Organometallics* **2020**, *39*, 361–373.
- [26] C. Zappelli, G. Ciancaleoni, S. Zacchini, F. Marchetti, *Organometallics* **2023**, *42*, 615–626.
- [27] K. Takatsu, R. Shintani, T. Hayashi, *Angew. Chem. Int. Ed.* **2011**, *50*, 5548–5552.
- [28] M. Takeda, K. Nagao, H. Ohmiya, *Angew. Chem. Int. Ed.* **2020**, *59*, 22460–22464.
- [29] T. Thaima, F. Zamani, C. J. T. Hyland, S. G. Pyne, *Synthesis* **2017**, *49*, 1461–1480.
- [30] M. L. Shegavi, S. Kumar Bose, *Catal. Sci. Technol.* **2019**, *9*, 3307–3336.
- [31] R. J. Newland, J. M. Lynam, S. M. Mansell, *Chem. Commun.* **2018**, *54*, 5482–5485.
- [32] M. W. Drover, L. L. Schafer, J. A. Love, *Angew. Chem. Int. Ed.* **2016**, *55*, 3181–3186.
- [33] J. B. Geri, N. K. Szymczak, *J. Am. Chem. Soc.* **2015**, *137*, 12808–12814.
- [34] R. Arévalo, C. M. Vogels, G. A. MacNeil, L. Riera, J. Péreza, S. A. Westcott, *Dalton Trans.* **2017**, *46*, 7750–7757.
- [35] A. Harinath, J. Bhattarjee, H. P. Nayek, T. K. Panda, *Dalton Trans.* **2018**, *47*, 12613–12622.
- [36] K. Nie, Y. Han, C. Wang, X. Cheng, *Appl. Organomet. Chem.* **2022**, *36*(3), e6570.
- [37] G. Zhang, H. Zeng, J. Wu, Z. Yin, S. Zheng, J. C. Fettinger, *Angew. Chem. Int. Ed.* **2016**, *55*, 14369–14372.
- [38] J. Guo, J. Chen, Z. Lu, *Chem. Commun.* **2015**, *51*, 5725–5727.
- [39] U. K. Das, C. S. Higman, B. Gabidullin, J. E. Hein, R. T. Baker, *ACS Catal.* **2018**, *8*, 1076–1081.
- [40] D. Mukherjee, A.-K. Wiegand, T. P. Spaniol, J. Okuda, *Dalton Trans.* **2017**, *46*, 6183–6186.
- [41] S. Raj Tamang, M. Findlater, *J. Org. Chem.* **2017**, *82*(23), 12857–12862.
- [42] X. Qi, T. Zheng, J. Zhou, Y. Dong, X. Zuo, X. Li, H. Sun, O. Fuhr, D. Fenske, *Organometallics* **2019**, *38*, 268–277.
- [43] S. Khoo, J. Cao, F. Ng, C.-W. So, *Inorg. Chem.* **2018**, *57*(20), 12452–12455.
- [44] T. Zhang, Y. Liu, B. Hu, C. Zhang, Y. Chen, Y. Liu, *Chin. Chem. Lett.* **2018**, *29*, 949–953.
- [45] A. Baishya, S. Baruah, K. Geetharani, *Dalton Trans.* **2018**, *47*, 9231–9236.
- [46] C. Chang Chong, R. Kinjo, *ACS Catal.* **2018**, *8*(2), 1076–1081.
- [47] G. Zhang, J. Cheng, K. Davis, M. G. Bonifacio, C. Zajackowski, *Green Chem.* **2019**, *21*, 1114–1121.
- [48] S. Lau, C. B. Provis-Evans, A. P. Jamesa, R. L. Webster, *Dalton Trans.* **2021**, *50*, 10696–10700.
- [49] M. L. Shegavi, A. Baishya, K. Geetharani, S. K. Bose, *Org. Chem. Front.* **2018**, *5*, 3520–3525.
- [50] Y.-J. Zhu, J.-J. Wang, J.-Y. Liad, T. Zhang, *Dalton Trans.* **2023**, *52*, 7581–7589.
- [51] M. Yu, C. Cui, N. Mookan, Z. Xiao, W. Zhong, *J. Mol. Struct.* **2024**, *1296*, 136840.
- [52] J. Luo, C. Cui, Z. Xiao, W. Zhong, C. Lu, X. Jiang, X. Li, X. Liu, *Dalton Trans.* **2022**, *51*, 11558–11566.
- [53] T. M. Maier, M. Gawron, P. Coburger, M. Bodensteiner, R. Wolf, N. P. van Leest, B. de Bruin, S. Demeshko, F. Meyer, *Inorg. Chem.* **2020**, *59*, 16035–16052.
- [54] Y. Zhang, T. Mei, D. Yang, Y. Zhang, B. Wang, J. Qu, *Inorg. Chem. Commun.* **2017**, *86*, 133–136.
- [55] C. M. M'thuruaine, H. B. Friedrich, E. O. Changamu, M. D. Bala, *Inorg. Chim. Acta* **2012**, *390*, 83–94.
- [56] L. Busetto, F. Marchetti, F. Renili, S. Zacchini, V. Zanotti, *Organometallics* **2010**, *29*, 1797–1805.
- [57] A. J. L. Pombeiro, *J. Organomet. Chem.* **2005**, *690*, 6021–6040.
- [58] A. I. F. Venâncio, M. F. C. Guedes da Silva, L. M. D. R. S. Martins, J. J. R. Fraústo da Silva, A. J. L. Pombeiro, *Organometallics* **2005**, *24*, 4654–4665.
- [59] G. Agonigi, G. Ciancaleoni, T. Funaioli, S. Zacchini, F. Pineider, C. Pinzino, G. Pampaloni, V. Zanotti, F. Marchetti, *Inorg. Chem.* **2018**, *57*, 15172–15186.
- [60] C. P. Gordon, C. Raynaud, R. A. Andersen, C. Copéret, O. Eisenstein, *Acc. Chem. Res.* **2019**, *52*, 2278–2289.
- [61] L. Busetto, V. Zanotti, *J. Organomet. Chem.* **2005**, *690*, 5430–5440.
- [62] M. Krejčík, M. Daněk, F. Hartl, *J. Electroanal. Chem.* **1991**, *317*, 179–187.
- [63] F. M. Al-Qaisi, A. K. Qaroush, A. H. Smadi, F. Alsoubani, K. I. Assaf, T. Repo, A. F. Eftaiha, *Dalton Trans.* **2020**, *49*, 7673–7679.
- [64] N. H. Kim, E. Y. Seong, J. H. Kim, S. H. Lee, K.-H. Ahn, E. J. Kang, *J. CO₂ Util.* **2019**, *34*, 516–521.
- [65] A. J. Kamphuis, F. Picchioni, P. P. Pescarmona, *Green Chem.* **2019**, *21*, 406–448.
- [66] S. Wang, C. Xi, *Chem. Soc. Rev.* **2019**, *48*, 382–404.
- [67] V. G. Albano, L. Busetto, M. Monari, V. Zanotti, *J. Organomet. Chem.* **2000**, *606*, 163–168.
- [68] F. Menges, “Spectragraph - optical spectroscopy software”, Version 1.2.5, @ 2016–2017, <http://www.effemm2.de/spectragraph>.
- [69] G. R. Fulmer, A. J. M. Miller, N. H. Sherden, H. E. Gottlieb, A. Nudelman, B. M. Stoltz, J. E. Bercaw, K. I. Goldberg, *Organometallics* **2010**, *29*, 2176–2179.
- [70] R. K. Harris, E. D. Becker, S. M. Cabral De Menezes, R. Goodfellow, P. Granger, *Pure Appl. Chem.* **2001**, *73*, 1795–1818.
- [71] W. Willker, D. Leibfritz, R. Kerssebaum, W. Bermel, *Magn. Reson. Chem.* **1993**, *31*, 287–292.
- [72] G. M. Sheldrick, SADABS-2008/1 - Bruker AXS Area Detector Scaling and Absorption Correction, Bruker AXS: Madison, Wisconsin, USA, **2008**.
- [73] G. M. Sheldrick, *Acta Crystallogr. Sect. C* **2015**, *71*, 3–8.

Manuscript received: May 2, 2024

Accepted manuscript online: June 11, 2024

Version of record online: July 24, 2024

[Correction added on 23 December 2024, after first online publication: The copyright line was changed.]